AGU PUBLICATIONS

Geochemistry, Geophysics, Geosystems

RESEARCH ARTICLE
10.1002/2014GC005622

Key Points:
- IR and Raman spectroscopies were used for detecting heat signatures along fault
- Record of high temperature (700°C) was observed in the Taiwan Chelungpu fault
- Decomposition and aromatization reactions occurred during earthquake slip

Supporting Information:
- Supporting Information S1

Correspondence to:
T. Hirono,
hirono@ess.sci.osaka-u.ac.jp

Citation:
Hirono, T., Y. Maekawa, and H. Yabuta (2015), Investigation of the records of earthquake slip in carbonaceous materials from the Taiwan Chelungpu fault by means of infrared and Raman spectroscopies, *Geochem. Geophys. Geosyst.*, *16*, 1233–1253, doi:10.1002/2014GC005622.

Received 17 OCT 2014
Accepted 5 APR 2015
Accepted article online 9 APR 2015
Published online 2 MAY 2015

Investigation of the records of earthquake slip in carbonaceous materials from the Taiwan Chelungpu fault by means of infrared and Raman spectroscopies

Tetsuro Hirono[1], Yuka Maekawa[1], and Hikaru Yabuta[1]

[1]Department of Earth and Space Science, Graduate School of Science, Osaka University, Toyonaka, Osaka, Japan

Abstract To understand the mechanism of fault lubrication during the 1999 Taiwan Chi-Chi earthquake, we developed a new temperature proxy for carbonaceous materials by using infrared and Raman spectroscopies together with heating and friction experiments. We found marked anomalies in the infrared and Raman spectra of carbonaceous materials retrieved from the primary slip zone of the earthquake: the infrared spectra exhibited very weak aliphatic CH_2 and CH_3 peaks and aromatic C=C absorbance peaks, and the Raman spectra exhibited very weak disordered and graphitic bands and a high ratio of disordered band area to graphitic band area. Those weak peaks and bands and the band area ratio were reproduced by heating carbonaceous materials from the nearby host rock to 700°C. These results suggest that the frictional heat in the slip zone reached approximately 700°C. We characterized the host rock's carbonaceous materials by means of elemental analysis, pyrolysis-gas chromatography-mass spectrometry, and simultaneous thermogravimetry-differential scanning calorimetry and found that the H/C and O/C ratios were 1.29 and 0.30, respectively (which are close to the ratios for lignin) and that the volatile fraction was as high as 48 wt %. The pyrolysates obtained by heating from 100 to 400°C were dominated by phenols, fatty alcohols, and *n*-alkanes. When the residue from pyrolysis at 100–400°C was rapidly heated to 700°C, the resulting pyrolysate was dominated by phenols, aromatic compounds, heterocyclic compounds, and *n*-alkenes. This information suggests that change in the infrared and Raman spectra with increasing temperature may have been due to decomposition and aromatization reactions during pyrolysis. Rapid heating during earthquake slip may promote reactions of carbonaceous materials that are different from the reactions that occur during long-term geological metamorphism.

1. Introduction

The 1999 Taiwan Chi-Chi earthquake (M_w 7.6), the largest inland earthquake recorded in Taiwan in the twentieth century, had its hypocenter at 23.853°N and 120.816°E and a focal depth of 8 km on the southern region of the Chelungpu fault [*Ma et al*., 1999]. The earthquake propagated both updip and laterally northward for about 100 km along the fault, producing surface ruptures [*Ma et al*., 2000; *Chen et al*., 2001; *Lee et al*., 2003]. The largest ground velocity and displacement (up to 3 m s^{-1} and 8 m, respectively) were recorded at the northern end, whereas the level of high-frequency radiation was lower at the northern end than at the southern end [*Shin and Teng*, 2001]. Investigation of the faulting mechanism and the temperature of the fault, which are related to the levels of friction and shear stress on the fault, is crucial because some faulting mechanisms—such as thermal pressurization, in which fluid pressure generated by shear-related heating reduces the fault strength during slip [*Sibson*, 1973]—are promoted by frictional heating.

Various temperature proxies have been used for samples from the Chelungpu fault. For example, thermomagnetic analysis showed that at high temperature (≥400°C), thermal decomposition of paramagnetic minerals cause magnetite formation [*Mishima et al*., 2009; *Chou et al*., 2012], which coincides with the observed high magnetic susceptibility in the fault [*Hirono et al*., 2006, 2007a]. Geochemical and isotope analyses showed marked anomalies in the concentrations of fluid-mobile trace elements (Sr, Cs, Rb, and Li) and in the Sr isotope ratios in the fault, indicating that a high-temperature fluid (≥350°C) was present during the earthquake [*Ishikawa et al*., 2008]. Clay mineral analysis showed the disappearances of chlorite and kaolinite and a marked decline in the amount of illite in the fault, and the temperature in the fault was estimated to have reached 900–1100°C, as indicated by comparison of the microstructures in the fault and in heated

host-rock samples [*Kuo et al*., 2009, 2011]. Inorganic carbon content was found to be low in the fault [*Ikehara et al*., 2007], and Arrhenius equation-based evaluation of the kinetics of the thermal decomposition of calcite suggested that the temperature reached in response to frictional heating during the Chi-Chi earthquake was approximately 900°C [*Hirono et al*., 2007b].

However, temperature determinations by means of these proxies are subject to various uncertainties. Both the thermomagnetic analysis and geochemical and isotope analyses suggested that the lower limit of frictional heating was $\geq$400°C. The temperatures of 900–1100 and 900°C estimated from the dehydration (dehydroxylation) and decarbonation reactions, respectively, are probably unreliable because these reactions can be affected by reversible reactions, dissolution, and recrystallization. Therefore, we focus on the irreversible maturation of carbonaceous materials induced by heating. Vitrinite reflectance is widely used as a geothermometer not only by petroleum geologists but also by structural geologists [*Bustin*, 1983; *Sakaguchi*, 1996; *Mukoyoshi et al*., 2006], because it is sensitive to temperature and increases irreversibly when vitrinite is exposed to high temperature. In samples from the Chelungpu fault, *Sakaguchi et al*. [2007] and *Maekawa et al*. [2014] have already reported high values of the reflectance in the fault. However, *Kitamura et al*. [2012] suggested that the commonly used kinetic model for vitrinite reflectance [*Sweeney and Burnham*, 1990] does not yield accurate estimates of the peak temperature in a fault zone; *Kitamura et al*. [2012] based this suggestion on comparisons between the measured temperature during high-velocity friction experiments with coal and the calculated temperature from the measured value of vitrinite reflectance in an experimental specimen.

In this study, we therefore developed a different temperature proxy for carbonaceous materials by using infrared (IR) and Raman spectroscopies. Over the last half-century, both techniques have been used to characterize the chemical structures of carbonaceous materials such as coal, oil shale, maceral, kerogen, and graphite. As early as the 1960s, IR spectroscopy was used for the chemical characterization of such materials [*Bent and Brown*, 1961; *Czuchajowski*, 1961; *Painter et al*., 1978], and micro-Fourier transform infrared spectroscopy allowed their characterization on the microscale [e.g., *Landais and Rochdi*, 1990; *Rochdi and Landais*, 1991]. Fourier transform IR has also been used to determine the rank (maturity) of coals and petroleum source rocks [e.g., *Lin and Ritz*, 1993; *Mastalerz and Bustin*, 1993], to identify the specific functional groups in and estimate the thermal metamorphism grade of organic matter in a chondritic meteorite [e.g., *Hayatsu et al*., 1977; *Matrajt et al*., 2004], and to detect the record of frictional heat in a fault [*Hirono et al*., 2014].

Raman spectroscopy has been used to characterize the chemical structures of coals [*Tuinstra and Koenig*, 1970] and to determine the maturity of coals and other organic matter, as well as to explore their coalification, carbonization, and graphitization [e.g., *Friedel and Carlson*, 1972; *Green et al*., 1983; *Kelemen and Fang*, 2001]. The use of Raman spectroscopy of natural carbonaceous materials and graphite as a geothermometer has been explored by comparing with metamorphic grade [*Pasteris and Wopenka*, 1991; *Wopenka and Pasteris*, 1993], and this technique has been used in many studies of metamorphic geology [e.g., *Jehlicka and Beny*, 1992; *Yui et al*., 1996; *Beyssac et al*., 2002; *Rahl et al*., 2005]. Progress on the use of Raman spectroscopy for coal research has been reviewed by *Potgieter-Vermaak et al*. [2010]. Furthermore, Raman spectroscopy has recently been used in meteorite research to estimate the thermal metamorphic grade of organic matter in a chondrite [e.g., *Quirico et al*., 2003, 2009; *Bonal et al*., 2006; *Busemann et al*., 2007] and in earthquake research to investigate the frictional heat record in a fault [*Hirono et al*., 2009]. These previous studies indicate that IR and Raman spectroscopies can be expected to be useful for characterizing the chemical structure of carbonaceous materials not only for petroleum research but also for fault-rock research related to earthquake slip.

Here, we used IR and Raman spectroscopies to analyze both carbonaceous materials retrieved from Chelungpu fault samples and the products of heating and friction experiments. On the basis of our results, we make inferences about the processes that effected the observed changes in the carbonaceous materials, and we discuss the frictional heat generated during the Chi-Chi earthquake along with the values of several other parameters related to frictional heating.

2. Materials and Methods

2.1. Sample Description

During the Taiwan Chelungpu-Fault Drilling Project, which began in 2002, the Chelungpu fault was penetrated (Figure 1a), and core samples were recovered from two main holes, Hole A (total depth, 2003.00 m)

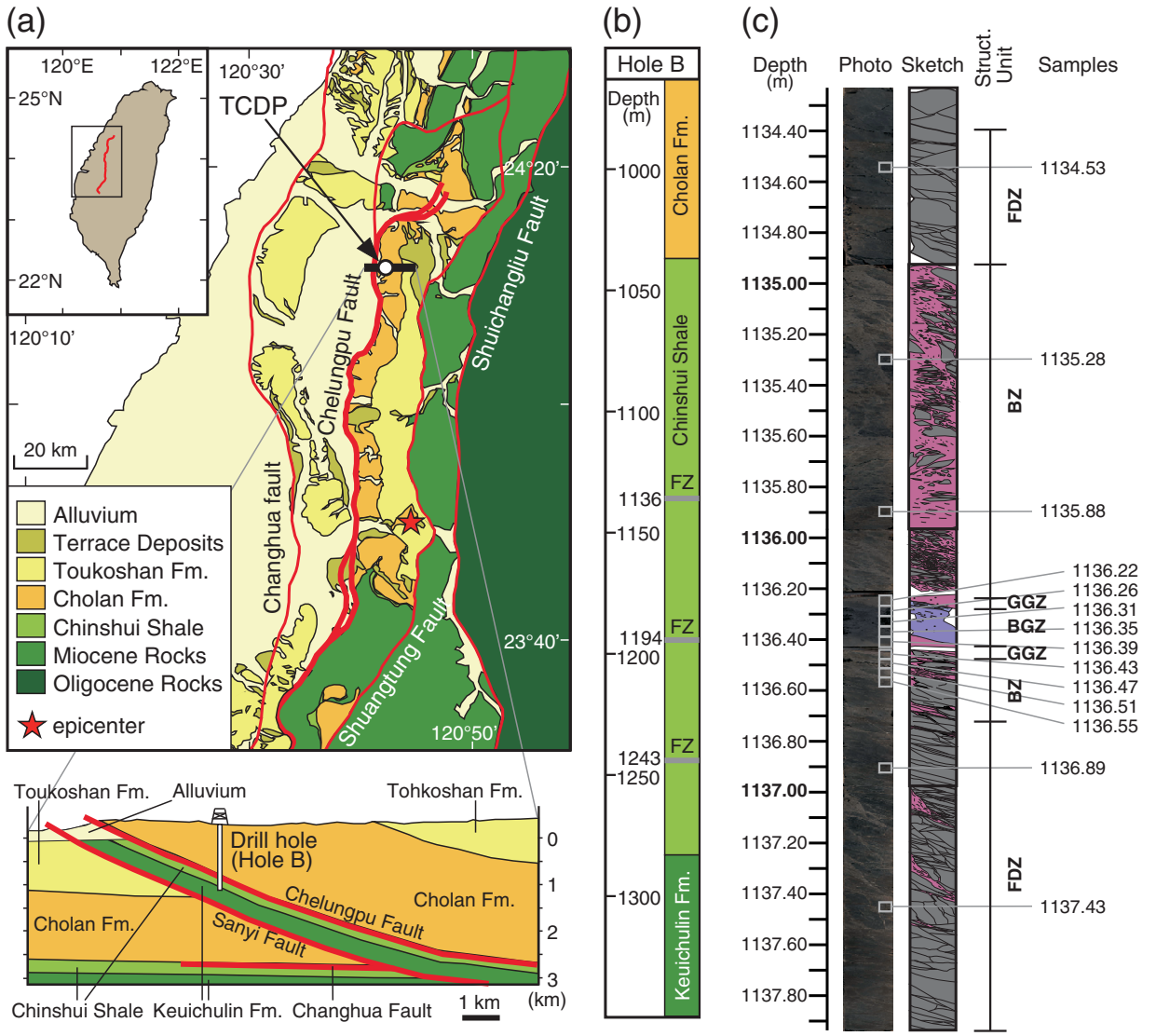

Figure 1. (a) Geological map of central Taiwan showing an east-west cross section through the drill hole site and the site of the Taiwan Chelungpu-Fault Drilling Project (TCDP), (b) geological column from Hole B showing the three dominant fault zones (at depths of 1136, 1194, and 1243 m), and (c) core photo and interpretive sketch of the shallowest fault zone. In Figure 1c, the small boxes on the core photo indicate the sampling points for carbonaceous material analyses. FZ, fault zone; FDZ, fracture-damaged zone; BZ, breccia zone; GGZ, gray gouge zone; and BGZ, black gouge zone.

and Hole B (total depth, 1352.60 m), and from one side-track hole (Hole C). In Hole B core samples, three dominant fault zones, FZB1136 (fault zone around 1136 m depth in Hole B), FZB1194, and FZB1243, were observed within the Chinshui Shale (Figure 1b) and interpreted as segments of the Chelungpu fault [*Hirono et al.*, 2006, 2007a, 2008]. The shallowest fault zone was most likely the one that slipped during the Chi-Chi earthquake, as indicated by evidence of recent heating and a major stress-orientation anomaly in that zone [*Kano et al.*, 2006; *Lin et al.*, 2007; *Wu et al.*, 2007].

The following subzones were encountered in FZB1136, from top to bottom (Figure 1c): upper fracture-damaged zone (1134.40–1134.93 m), upper breccia zone (1134.93–1136.22 m), upper gray gouge zone (1136.22–1136.26 m), black gouge zone (1136.26–1136.40 m), lower gray gouge zone (1136.40–1136.46 m), lower breccia zone (1136.46–1136.70 m), and lower fracture-damaged zone (1136.70–1137.90 m). The primary slip zone (PSZ) during the Chi-Chi earthquake was identified as a millimeter-thick shear zone within the black gouge zone at 1136.38 m depth, on the basis of the fact that neoformed magnetite in the black gouge at that depth carries a stable paleomagnetic component consistent with the 1999 international geomagnetic reference field dipole magnetic vector [*Chou et al.*, 2012].

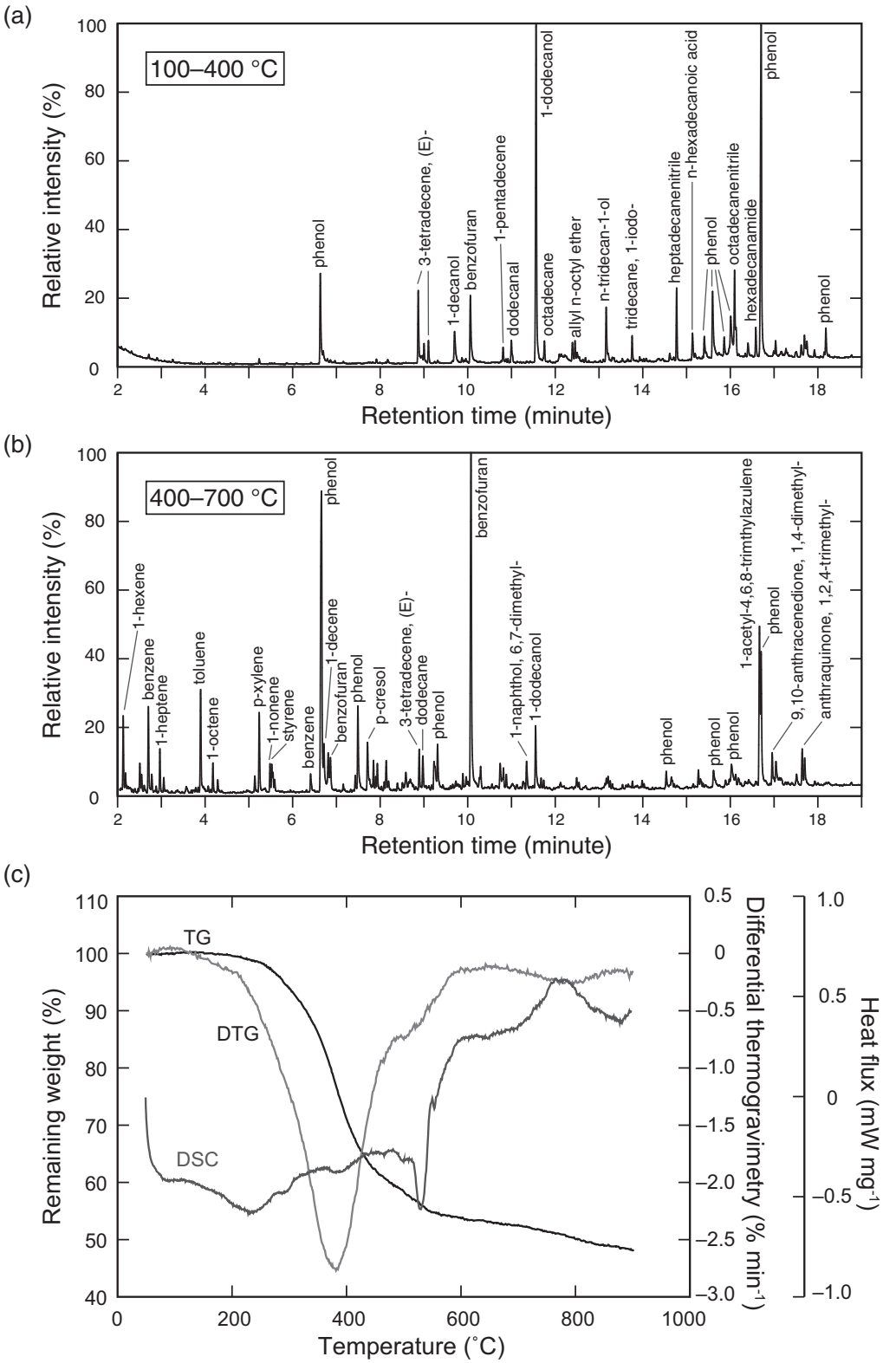

Figure 2. Pyrograms and thermoanalytical profiles of the carbonaceous materials from the host-rock samples: (a) pyrogram obtained by heating from 100 to 400°C, (b) pyrogram obtained by rapidly heating to 700°C the residue left after pyrolysis at 400°C, and (c) thermogravimetry (TG), differential TG (DTG), and differential scanning calorimetry (DSC) curves over the temperature range of 50–900°C.

We collected 16 subsamples from the FZB1136 core sample (Figure 1c). Carbonaceous materials in the samples were extracted by means of a CsF-HF technique [*Cody et al*., 2002; *Cody and Alexander*, 2005; *Alexander et al*., 2007]. The samples were first treated with 2 N HCl to remove metal, sulfide, and carbonate and were then rinsed with Milli-Q water several times. The rinsed samples were treated with two immiscible liquids, dioxane and an aqueous CsF-HF solution (1.6–1.7 g mL^{-1} and pH 5–7). The carbonaceous materials liberated by this treatment were collected at the interface between the two phases; rinsed in succession with 2 N HCl, 1 N HCl-9 N HF, 2 N HCl, Milli-Q water, and methanol; dried at 40–60°C for 12 h; and finally mounted in synthetic resin. The recovery percentages of the carbonaceous materials from the samples were 0.06–0.46 wt %.

2.2. Characterization of the Host-Rock's Carbonaceous Materials

The atomic composition of the carbonaceous materials retrieved from a host-rock subsample collected from the Chinshui Shale at 1104.76 m depth in Hole A of the Taiwan Chelungpu-Fault Drilling Project was determined with a CHNS-O elemental analyzer (EA3000, EuroVector, Italy) and was as follows: 33.96 ± 4.38 wt % C, 3.67 ± 0.38 wt % H, and 13.59 ± 0.43 wt % O. The atomic H/C and O/C ratios were 1.29 and 0.30, respectively, which correlate well with the atomic characteristics of lignin [*Payne and Ortoleva*, 2001], which is the primitive substance for terrigenously derived kerogen (Type III on the van Krevelen diagram).

To characterize the host-rock's carbonaceous materials on the molecular level, we used pyrolysis-gas chromatography-mass spectrometry (pyrolysis GC/MS) on a Multi-Shot Pyrolyzer (Py-3030D, Frontier Lab, Japan; furnace temperature 700°C, interface temperature 300°C) directly coupled to a gas chromatograph-mass spectrometer (GCMS-QP2010 Ultra, Shimadzu, Japan) equipped with an Rtx-5MS column (30 m length, 0.25 mm inner diameter, 0.25 μm film thickness; Restek, Pennsylvania). Approximately 1 mg of the carbonaceous materials was heated from 100 to 400°C at a rate of 50°C min^{-1} under vacuum, and the gas-phase pyrolysates that were collected in a cryotrap were analyzed by GC/MS. The residue was again heated rapidly to 700°C, and the resulting pyrolysates were also analyzed by GC/MS. For the CG/MS analysis, helium was used as the carrier gas at a flow rate of 1 mL min^{-1}, and the split ratio was 50. The injection temperature was 300°C, and the column temperature program was as follows: hold at 40°C for 2 min, heat to 310°C at 15°C min^{-1}, and hold at 310°C for 10 min. The mass spectrometer was operated in the electron ionization mode (70 eV, scan range *m/z* 35–600, scan interval 0.2 s), and the ion source temperature was kept at 230°C. The pyrolysates were identified by comparing their mass spectra with those of standards reported in the library of the National Institute of Standards and Technology. The pyrolysates from the first shot (100–400°C, Figure 2a) were dominated by phenols, fatty alcohols, and octadecane, whereas those from the second shot (400–700°C, Figure 2b) were dominated by phenols and other aromatic compounds, heterocyclic compounds, and *n*-alkenes. Sulfur dioxide and carbon disulfide were detected in the second-shot pyrolysates at retention times of 1.437 and 1.837 s, respectively (not shown in Figure 2b).

To thermochemically characterize the host-rock's carbonaceous materials, we used simultaneous thermogravimetry (TG)-differential scanning calorimetry (DSC). Approximately 2 mg of the carbonaceous materials was placed in a covered $Pt_{90}Rh_{10}$ crucible and heated from room temperature to 900°C at a rate of 20°C min^{-1} under a flow of Ar gas (50 mL min^{-1}); the mass and heat were monitored with a STA 449 C Jupiter balance (Netzsch, Germany). The resultant TG-DSC curves, showing the weight lost with increasing temperature and the heat required for the reaction, respectively, are shown in Figure 2c together with the differential TG curve. Mass loss started at approximately 250°C and reached 48% at 900°C, and a large differential TG peak was observed at around 380°C. The DSC curve showed broad, shallow endotherms in the 200–400°C temperature range; a shift to exothermicity was observed at $\geq$400°C, and a broad exothermic peak at around 770°C was observed, along with a sharp endothermic peak at 530°C.

2.3. Heating and Friction Experiments

Because fault slip during an earthquake is expected to affect the chemical structure of carbonaceous materials, we heated carbonaceous materials retrieved from the host-rock subsamples described in section 2.2. A TG-DSC apparatus (STA 449 C Jupiter balance) was used to heat the extracted carbonaceous materials to 100, 300, 400, 500, 700, or 900°C at a rate of 10°C min^{-1} under an Ar or air atmosphere. Because the heating rate during an earthquake is several tens to several hundreds of degrees Celsius per second, we also performed two experiments at a heating rate of 500°C min^{-1} under Ar (the target temperatures were 280 and 400°C).

Table 1. Conditions for the Heating and Friction Experiments

	Run Number	Maximum Temperature (°C)	Atmosphere	Heating Rate (°C min^{-1})	Normal Stress (MPa)	Displacement (m)	Slip Rate (m s^{-1})
Heating Exp.	H001	100	Ar	10			
	H002	300	Ar	10			
	H003	400	Ar	10			
	H004	500	Ar	10			
	H005	700	Ar	10			
	H006	900	Ar	10			
	H011	100	Air	10			
	H012	300	Air	10			
	H013	400	Air	10			
	H014	500	Air	10			
	H015	700	Air	10			
	H016	900	Air	10			
	H101	280	Ar	500			
	H102	400	Ar	500			
Friction Exp.	HVR2957	40	Air		1.0	5.0	0.01
	HVR2919	120	Air		1.0	5.0	0.1
	HVR2956	250	Air		1.0	16.0	1

A rotary shear apparatus was used to produce shear damage to the carbonaceous materials (supporting information Figure S1). Approximately 500 mg of dry powdered host rock was placed between the ends of two cylinders of gabbro (25 mm diameter) and sealed in a polytetrafluoroethylene sleeve to prevent leaks. The experiments were performed at ambient humidity at a velocity of 0.01, 0.1, or 1 m s^{-1} with 5–16 m of displacement under 1 MPa of normal stress, and temperature during the experiments was measured with a thermocouple set in the stationary side of the apparatus. After the friction experiments, the shear-damaged powdered host rock at the outer 12.5–7.5 mm was corrected, and the carbonaceous materials were extracted from it by means of the CsF-HF technique mentioned above. The experimental conditions are summarized in Table 1. Although the heating rate and duration and the level of friction applied to the samples in these experiments do not replicate the conditions in the fault zone during the Chi-Chi earthquake, the experimental results enabled us to qualitatively discuss the effects of heating and friction on the chemical structure of carbonaceous materials.

2.4. IR Spectroscopy

The IR absorption spectra of carbonaceous materials generally show the following absorbance peaks [e.g., *Painter et al*., 1981; *Lin and Ritz*, 1993; *Stuart*, 2004]: a broad peak at around 3400 cm^{-1}, attributed to O–H stretching of absorbed H_2O, =C–H stretching of alkyne groups, phenol O–H stretching, and carboxylic O–H stretching; sharp peaks at 2960, 2930, and 2860 cm^{-1}, attributed to asymmetrical CH_3 stretching, asymmetrical CH_2 stretching, and symmetrical CH_2 stretching vibrations, respectively; a band at around 2370–2345 cm^{-1}, attributed to atmospheric CO_2; a peak at 1680 cm^{-1}, attributed to C=O stretching of carbonyl groups; a peak at around 1600–1580 cm^{-1}, attributed to aromatic ring C=C stretching; sharp peaks at 1455 and 1375 cm^{-1}, attributed to asymmetrical CH_3 bending and symmetrical CH_2 bending vibrations, respectively; and other weak peaks at around 1500–1000 cm^{-1} (the fingerprint region), attributed to various bending vibrations of complicated functions.

The CH_2/CH_3 ratio (2930 cm^{-1}/2960 cm^{-1}) is sensitive to the degree of carbon skeletal branching and to the length of aliphatic chains [e.g., *Lin and Ritz*, 1993; *Mastalerz and Bustin*, 1996; *Flynn et al*., 2003]: a relatively low CH_2/CH_3 ratio corresponds to relatively high maturity and a high degree of carbon skeletal branching or short aliphatic chains, and has been used as a proxy for kerogen and coal maturity [e.g., *Ibarra et al*., 1996]. *Huang and Otten* [1998] demonstrated experimentally that the CH_3/CH_2 ratio (2956 cm^{-1}/2920 cm^{-1}), that is, the reciprocal of the CH_2/CH_3 ratio, of Green River kerogen increases with the duration of heating at temperatures of ≥380°C, owing to thermal cracking of aliphatic chains. In addition, experimental heating of insoluble organic matter in the Murchison meteorite showed that the peaks for both aliphatic asymmetrical CH_3 and CH_2 stretching vibrations decrease with the duration of heating at temperatures of ≥240°C, owing to the breaking of aliphatic side chains [*Kebukawa et al*., 2010]. In contrast, *Guo and Bustin* [1998] experimentally demonstrated that the ratio of peaks for aliphatic CH absorption at 3000–2800 cm^{-1}

to peaks for aromatic C=C absorption at 1650–1520 cm^{-1} in Western Canadian Cretaceous coals decreased with the duration of heating at temperatures of ≥320°C. The CH_2/C=C peak ratio (2930 cm^{-1}/1600 cm^{-1}) in immature kerogen retrieved from middle Holocene peat strata (Zhanjian, Guangdong Province, China) decreased when the kerogen was heated at temperatures of ≥350°C [*Zeng and Wu*, 2007], and the ratio in the Murchison meteorite insoluble organic matter also appeared to decrease at 260°C in an isothermal heating experiment [*Kebukawa et al*., 2010].

We obtained IR absorption spectra of our carbonaceous materials on a CaF_2 plate by using a Fourier transform IR microspectrometer (FT/IR-6100 + IRT-3000, Jasco, Japan) with a ceramic IR light source, a germanium-coated KBr beam splitter, a mercury-cadmium-telluride detector, and 16-power Cassegrainian mirrors. One hundred IR transmission spectral scans were accumulated with a wavenumber resolution of 4 cm^{-1}, in the wavenumber range of 4000–1000 cm^{-1}, with a 50 × 50 μm^2 aperture. Spectra were obtained for 10 points on each sample. Background spectra were acquired for a blank CaF_2 plate adjacent to the targeted sample. To determine the CH_2/CH_3 and CH_2/C=C peak ratios, we measured the peak heights at 2930 and 2960 cm^{-1} with a linear baseline at 3000–2800 cm^{-1} and the peak height at 1600 cm^{-1} with a linear baseline at 1800–1500 cm^{-1}.

2.5. Raman Spectroscopy

The Raman spectrum of coal was first reported by *Tuinstra and Koenig* [1970]; the spectrum showed broad bands at 1575–1620 and 1355–1380 cm^{-1}, which are referred to as the G (graphitic) and D (disordered) bands. The subject of much research and debate, the G and D bands are considered to be attributable to the E_{2g} graphite mode with D^4_{6h} crystal symmetry and to the in-plane defects located between the basic structural units, respectively [e.g., *Potgieter-Vermaak et al*., 2010]. The ratio of the D and G band intensities (I_D and I_G, respectively) has been reported to be linearly correlated with the in-plane crystalline size of the hexagonal plane of aromatic layers, as determined by means of X-ray diffraction analysis [*Tuinstra and Koenig*, 1970]. *Jehlicka and Beny* [1992] reported that the I_D/I_G ratio of kerogens in various metamorphic rocks (pumpellyite to staurolite zones) decreases with the grade of metamorphism, and attributed the decreases to inverse correlation with the extent of crystallite size. *Wopenka and Pasteris* [1993] also showed that the I_D/I_G ratio of carbonaceous materials in various metamorphic rocks (chlorite zone to granulite facies) decreases with the grade of metamorphism, and suggested that the Raman spectrum is sensitive to the degree of crystallinity of carbonaceous materials ranging from kerogen and coal to granulite-grade graphite. However, *Cuesta et al*. [1998] compared a large data set of in-plane crystalline sizes of carbon solids determined by X-ray diffraction and Raman spectrometry, and pointed out the possibility that crystallite size might be underestimated by Tuinstra and Koenig's formula for disordered carbons. In addition, *Li et al*. [2006] found that graphitic crystallite structures are absent in highly disordered carbonaceous materials such as the solid residues left after pyrolysis of brown coals (i.e., coal char), as indicated by X-ray diffraction results, and these investigators suggested that the band at 1580–1600 cm^{-1} in the solid residues should be assigned not to the E_{2g} mode of graphite but rather to the aromatic quadrant ring-breathing mode and that their D band cannot be due to disorder in graphite and should instead be assigned to disorder in fused benzene rings (more than six rings but fewer rings than in graphite). In their coal chars, the areas of the D and G bands as well as their intensities decreased with elevated temperature. The positions of the D and G bands in coals and cokes have been found to move to lower wavenumbers with increasing temperature [*Green et al*., 1983]. The width of the D band for coal chars decreases with increasing heat-treatment temperature [*Johnson et al*., 1986], and the widths of the D and G bands of carbonaceous materials in metamorphic rocks have been reported to decrease with the grade of metamorphism [*Wopenka and Pasteris*, 1993].

We obtained Raman spectra of our carbonaceous materials by using a Raman microspectrometer (XploRa, Horiba Jobin Yvon, Japan) with the 532 nm line of a Nd:YAG laser. Ten Raman spectral scans with an exposure time of 10 s each were accumulated in the shift range of 1000–1800 cm^{-1} relative to the laser wavelength with a wavenumber resolution of 0.9 cm^{-1} and a 5 μm laser spot size. We used low laser power on the targeted surface (0.13 mW) to avoid thermal damage to the samples. Spectra were obtained for 25 points on each sample. After a linear baseline correction for reduction of fluorescence interference, the band intensity, band area, peak position, and band width (full width at half maximum) of the D and G bands were determined by means of PeakFit 3.0 software (Systat, San Jose, CA, USA) with a Voigt function. As a reference, their peak intensities and positions were recorded only after baseline correction.

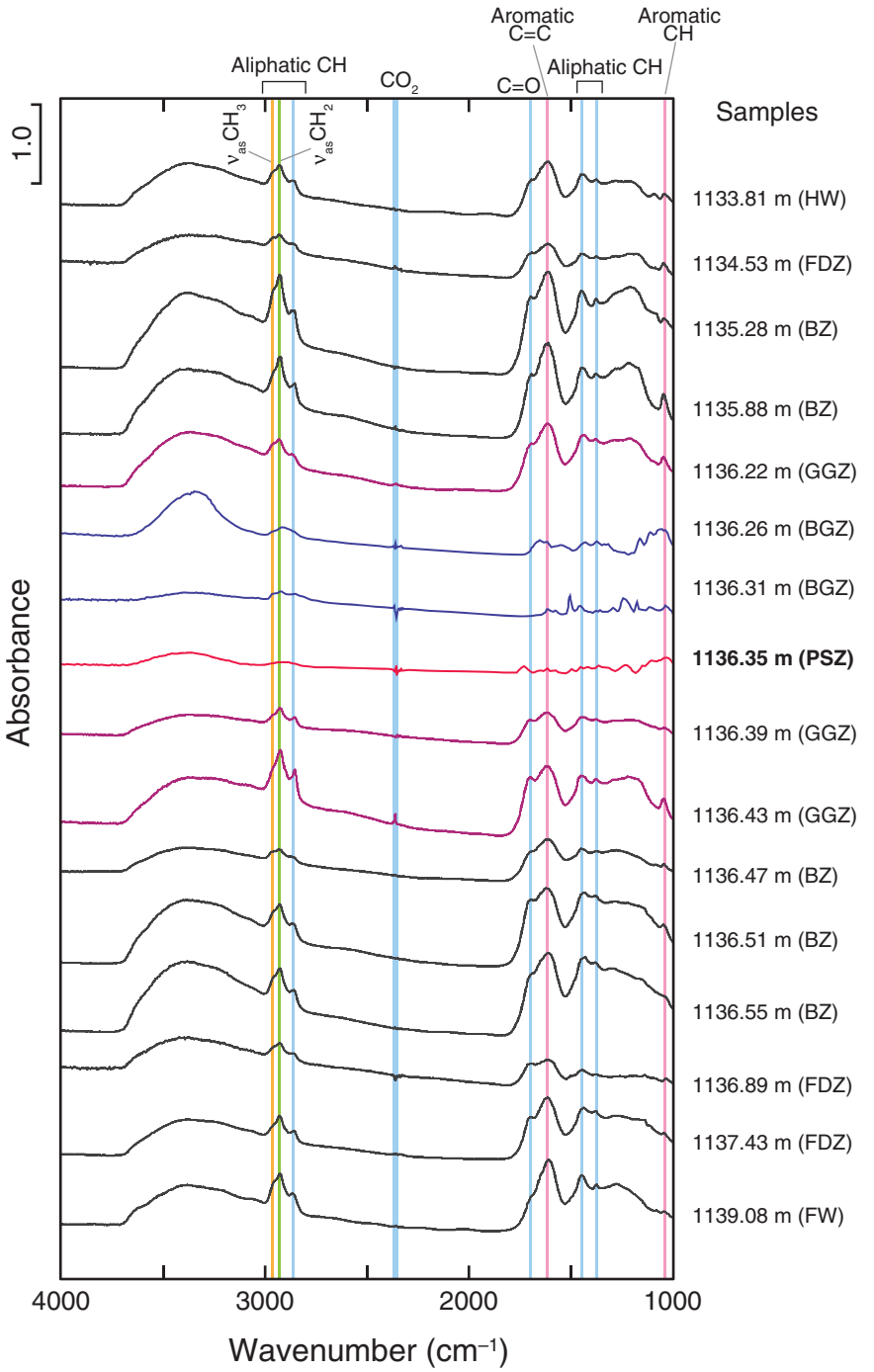

Figure 3. IR spectra of the carbonaceous materials retrieved from the Chelungpu fault and surrounding rocks. PSZ, primary slip zone; HW, hanging wall; FW, footwall; other abbreviations are defined in the caption of Figure 1.

3. Results

3.1. IR Spectra of Carbonaceous Materials From the Chelungpu Fault

The IR absorption spectra of all the carbonaceous materials extracted from the host rocks, fracture-damaged rocks, breccia samples, and gray gouge samples had sharp absorbance peaks at 2960, 2930, and 2860 cm^{-1}, which were attributed to asymmetrical CH_3 stretching, asymmetrical CH_2 stretching, and symmetrical CH_2 stretching vibrations, respectively (Figure 3), but the peaks of the PSZ and black gouge samples were very small. All the samples from the surrounding deformed rocks and intact host rocks exhibited

Table 2. Results of Infrared and Raman Spectroscopic Analyses for the Carbonaceous Materials Retrieved From the Taiwan Chelungpu Fault

Depth (m)	Structure	CH_2/CH_3	$CH_2/C{=}C$	I_D/I_G	A_D/A_G	ω_D (cm^{-1})	Γ_D (cm^{-1})	ω_G (cm^{-1})	Γ_G (cm^{-1})	R_o
1133.81	Upper host rock	1.54±0.13	0.53±0.32	0.76±0.03	1.39±0.14	1361.1±5.0	249.3±7.0	1598.0±1.2	97.2±11.4	0.57 ±0.22
1134.53	Fracture-damaged zone	1.51±0.15	0.52±0.07	0.69±0.02	1.43±0.06	1355.7±2.3	241.8±2.4	1599.8±0.6	79.7±4.6	0.63 ±0.21
1135.28	Breccia zone	1.44±0.06	0.84±0.11	0.75±0.02	1.46±0.10	1363.3±1.7	259.9±3.3	1597.2±1.2	94.1±4.6	0.45 ±0.12
1135.88	Breccia zone	1.56±0.14	0.55±0.09	0.74±0.06	1.63±0.28	1354.8±5.0	232.7±26.0	1598.8±1.2	79.3±11.2	0.63 ±0.20
1136.22	Gray gouge zone	1.51±0.17	0.48±0.15	0.74±0.05	1.42±0.14	1357.7±5.0	246.3±8.9	1599.1±1.2	89.8±11.9	0.64 ±0.22
1136.26	Black gouge zone	1.67±0.07	1.54±0.18	0.71±0.02	2.07±0.15	1352.7±0.8	255.7±3.2	1598.7±0.4	71.1±2.2	1.46 ±0.23
1136.31	Black gouge zone	1.78±0.40	2.69±1.02	0.74±0.04	2.04±0.31	1350.6±1.6	242.3±15.8	1597.8±1.4	71.8±6.5	1.19 ±0.35
1136.35	Primary slip zone	1.74±0.39	1.43±0.26	0.80±0.06	2.52±0.39	1346.7±4.5	188.4±42.8	1599.4±1.7	61.9±6.8	1.30 ±0.21
1136.39	Gray gouge zone	1.60±0.15	0.50±0.14	0.77±0.08	2.02±0.44	1352.8±4.4	210.3±34.4	1600.4±1.0	70.9±9.4	0.66 ±0.29
1136.43	Gray gouge zone	1.73±0.11	0.76±0.30	0.71±0.08	1.61±0.29	1351.7±6.7	225.2±22.2	1600.2±1.2	73.5±12.6	0.66 ±0.25
1136.47	Breccia zone	1.48±0.18	0.59±0.16	0.81±0.03	1.31±0.05	1362.9±1.9	248.6±3.2	1600.3±1.2	105.3±5.9	0.75 ±0.16
1136.51	Breccia zone	1.37±0.21	0.59±0.02	0.72±0.07	1.65±0.23	1353.5±6.0	231.3±27.9	1599.2±1.6	76.6±11.4	0.77 ±0.22
1136.55	Breccia zone	1.57±0.06	0.61±0.09	0.75±0.06	1.48±0.25	1357.6±4.9	245.0±13.0	1597.7±2.0	91.6±12.9	0.63 ±0.20
1136.89	Fracture-damaged zone	1.45±0.20	0.52±0.17	0.68±0.11	1.79±0.32	1347.2±6.9	227.8±32.8	1598.1±2.0	77.8±13.7	0.75 ±0.23
1137.43	Fracture-damaged zone	1.61±0.14	0.66±0.40	0.72±0.04	1.44±0.08	1360.3±5.5	248.6±8.8	1599.2±0.7	85.9±8.1	0.67 ±0.23
1139.08	Lower host rock	1.53±0.14	0.73±0.14	0.77±0.01	1.33±0.07	1361.4±1.4	250.0±3.7	1599.3±0.8	99.4±4.2	0.63 ±0.21

a sharp absorbance peak at 1680 cm^{-1}, which was attributed to C=O stretching, but this peak was not present in the spectra of the PSZ and black gouge samples. All the samples from the surrounding deformed/host rocks exhibited sharp absorbance peaks at 1600 and 1050 cm^{-1}, which were attributed to aromatic C=C stretching and aromatic in-plane C–H bending; these peaks were very weak in the spectra of the PSZ and black gouge samples. Weak absorbance peaks at 1455 and 1375 cm^{-1}, attributed to asymmetrical CH_3 bending and symmetrical CH_2 bending vibrations of aliphatic hydrocarbons, respectively, were observed in spectra of the surrounding deformed/host rocks but were extremely weak in the spectra of the PSZ and black gouge samples. Broad absorbances at around 3700–3000 cm^{-1}, attributable to the O–H stretching mode of H_2O molecules absorbed on the sample surface, to C=C–H stretching of alkene, or to phenol O–H stretching, were observed in the spectra of all the samples, but the absorbances of the PSZ and black gouge samples (at 1136.31 m) were very weak. Weak peaks at 1730 and 1250 cm^{-1}, which were attributed to C=O stretching and C–O stretching of aromatic esters, respectively [e.g., *Stuart*, 2004], were present only in the PSZ sample. The absorbance band at around 2370–2345 cm^{-1} was an artifact caused by exposure of the samples to atmospheric CO_2.

We calculated the CH_2/CH_3 and $CH_2/C{=}C$ peak ratios for all the samples (Table 2). The CH_2/CH_3 ratio for the PSZ sample was 1.74 ± 0.39, and the ratios for the black gouge samples were 1.67 ± 0.07 and 1.78 ± 0.40. However, the average of the ratios for the surrounding deformed/host rocks was 1.53 ± 0.09 (range, 1.37–1.73). The $CH_2/C{=}C$ ratio for the PSZ sample was 1.43 ± 0.26, and the ratios for the black gouge samples were 1.54 ± 0.18 and 2.69 ± 1.02; the average ratio for the surrounding deformed/host rocks was 0.60 ± 0.11 (range, 0.48–0.84).

3.2. Raman Spectra of Carbonaceous Materials From the Chelungpu Fault

The Raman spectra of all the extracted carbonaceous materials showed a broad band at around 1355 cm^{-1} (D band) and a band at 1600 cm^{-1} (G band), but these bands in spectra of the PSZ and black gouge samples were extremely weak compared with those in the spectra of the samples from the surrounding deformed/host rocks (Figure 4). Small shoulder peaks at around 1150, 1280, 1450, and 1700 cm^{-1} were observed in the spectra of the surrounding deformed/host rocks, whereas these peaks were not present in the spectra of the PSZ and black gouge samples. The peaks at around 1150 and 1450 cm^{-1} have been attributed to C–C stretching and CH_2 bending vibrations of aliphatic components [e.g., *Schneider et al*., 1979; *Lin-Vien et al*., 1991]. The peak at around 1280 cm^{-1} is attributable to the C–C interring stretching vibration of cyclic components [e.g., *Martin et al*., 2004; *Zhou et al*., 2012], and that at around 1700 cm^{-1} is attributable to C=O [e.g., *Lin-Vien et al*., 1991].

We determined the peak intensity ratios (I_D/I_G), band area ratios (A_D/A_G), peak positions (ω_D and ω_G), and full widths at half maximum (Γ_D and Γ_G) of the D and G bands for all the samples (shown in Table 2, along with the vitrinite reflectance data reported by *Maekawa et al*. [2014]). The I_D/I_G ratios for all the samples ranged from 0.68 to 0.81 (PSZ sample, 0.80 ± 0.06), but the A_D/A_G ratio for the PSZ sample (2.52 ± 0.39) was markedly higher than the ratios for the black gouge samples and the surrounding deformed/host rocks,

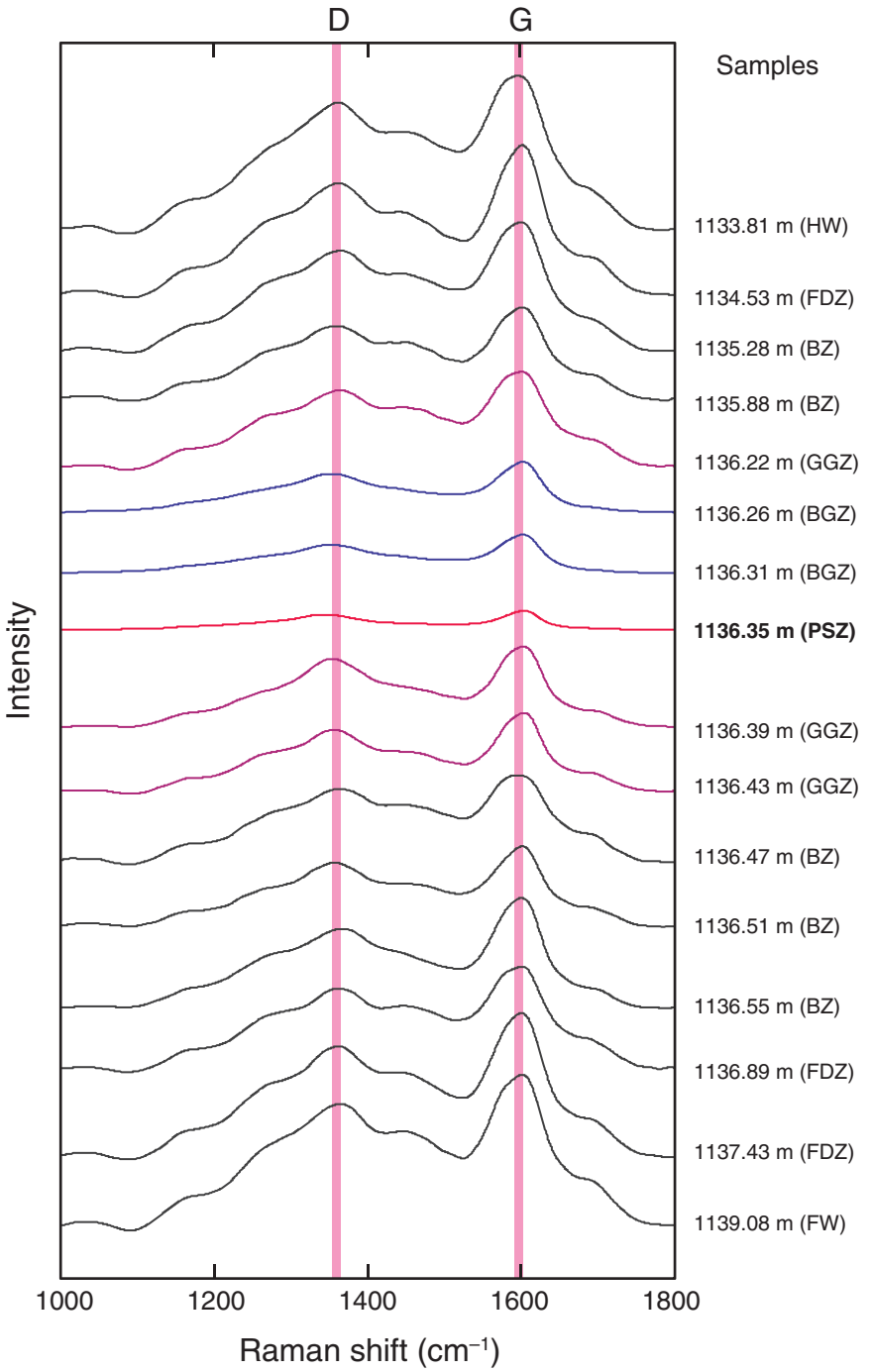

Figure 4. Raman spectra of the carbonaceous materials retrieved from the Chelungpu fault and surrounding rocks. D, disordered band; G, graphitic band; the other abbreviations are defined in the captions of Figures 1 and 3.

which ranged from 1.31 to 2.07. The ω_D value for the PSZ sample (1346.7 $\pm$ 4.5 cm^{-1}) was almost the same as the values for the black gouge samples (1352.7 $\pm$ 0.8 and 1350.6 $\pm$ 1.6 cm^{-1}) and the average value for the surrounding deformed/host rocks (1356.9 $\pm$ 4.9 cm^{-1}). The standard deviations of the Γ_D values for all the samples were large, but the Γ_D value for the PSZ sample (188.4 $\pm$ 42.8 cm^{-1}) was lower than the values for the black gouge samples and the values for the surrounding deformed/host rocks (range, 210.3–259.9 cm^{-1}). The ω_G value for the PSZ sample (1599.4 $\pm$ 1.7 cm^{-1}) was almost the same as the values for the black gouge samples (1598.7 $\pm$ 0.4 and 1597.8 $\pm$ 1.4 cm^{-1}) and the surrounding deformed/host rocks

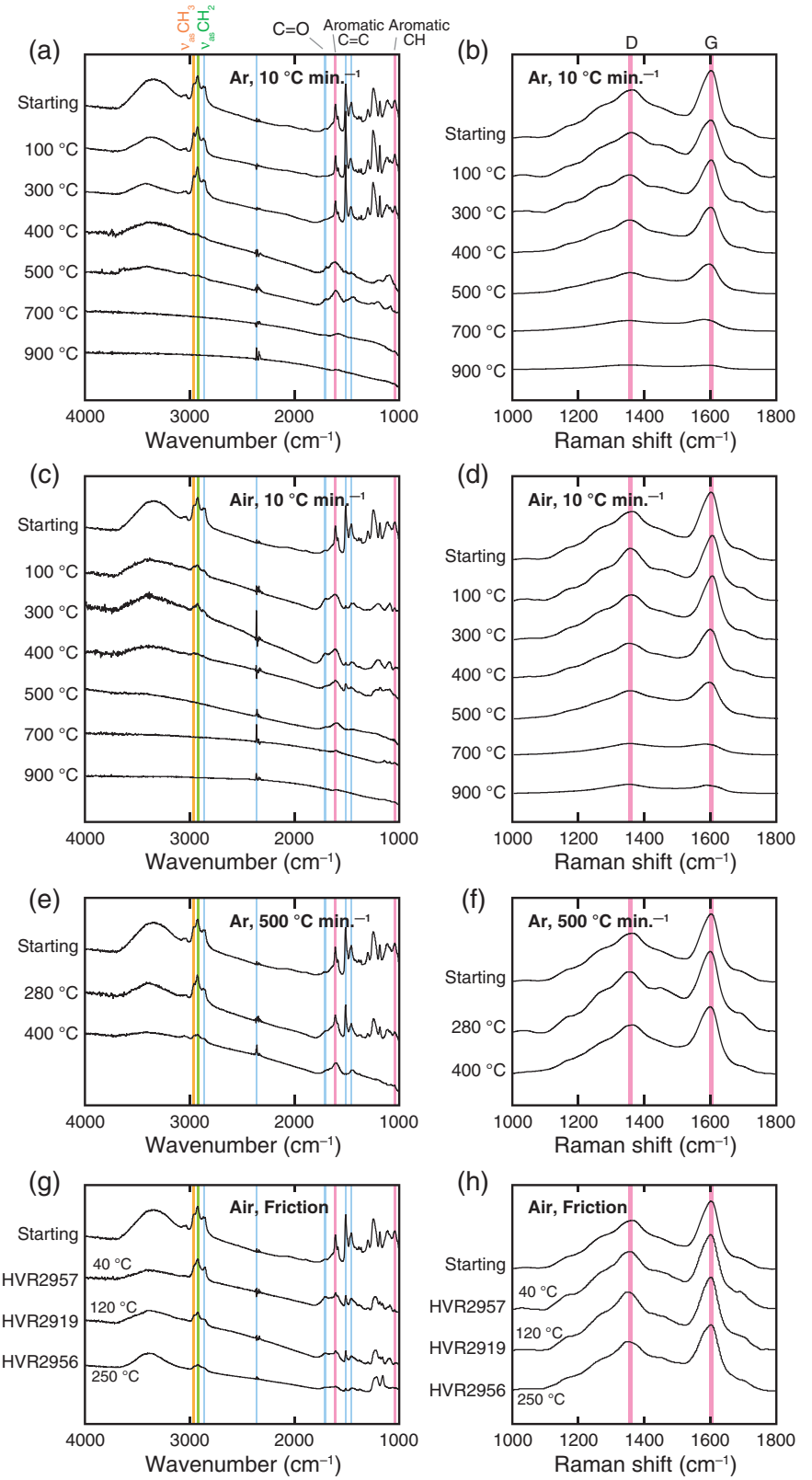

Figure 5. IR spectra (left column) and Raman spectra (right column) of the products of heating and friction experiments conducted on the carbonaceous materials: (a, b) heating experiment at a rate of 10°C min^{-1} under Ar, (c, d) heating experiment at a rate of 10°C min^{-1} in air, (e, f) heating experiment at a rate of 500°C min^{-1} under Ar, and (g, h) friction experiment in air.

Table 3. Results of Infrared and Raman Spectroscopic Analyses for the Carbonaceous Materials Retrieved From the Experiment Products

	Run Number	Maximum Temperature (°C)	CH_2/CH_3	$CH_2/C{=}C$	I_D/I_G	A_D/A_G	ω_D (cm^{-1})	Γ_D (cm^{-1})	ω_G (cm^{-1})	Γ_G (cm^{-1})
Heating Exp.[a]	H001	100	1.66±0.31	1.16±0.11	0.72±0.05	1.53±0.14	1356.5±4.0	248.8±9.7	1600.5±1.3	81.3±8.6
	H002	300	1.70±0.22	1.02±0.24	0.71±0.05	1.55±0.18	1355.2±4.2	252.1±8.5	1599.2±1.5	81.9±11.2
	H003	400	1.97±0.22	0.33±0.07	0.67±0.02	1.81±0.12	1359.2±3.7	274.2±8.0	1596.8±1.5	76.2±3.6
	H004	500	1.74±0.48	0.19±0.04	0.72±0.04	1.89±0.23	1363.7±4.6	285.9±9.6	1594.1±1.7	84.0±9.0
	H005	700		0.00±0.00	1.05±0.09	2.86±0.45	1364.6±4.1	287.5±17.2	1585.9±3.1	101.5±6.8
	H006	900			1.25±0.05	3.09±0.30	1359.5±2.6	265.6±14.2	1585.6±3.1	113.9±3.1
	H011	100	1.69±0.20	0.54±0.14	0.68±0.04	1.66±0.18	1352.7±3.6	245.7±11.0	1599.6±0.7	73.2±7.4
	H012	300	1.81±0.20	0.42±0.10	0.67±0.03	1.77±0.24	1351.6±4.8	251.4±19.1	1598.6±1.1	70.4±7.0
	H013	400	1.78±0.37	0.40±0.20	0.68±0.04	1.84±0.14	1358.6±5.4	276.8±7.9	1596.3±1.1	76.8±5.8
	H014	500	1.70±0.34	0.12±0.02	0.82±0.04	2.20±0.12	1363.9±4.2	287.1±10.4	1589.7±1.2	86.3±3.5
	H015	700		0.00±0.00	1.19±0.08	3.03±0.17	1363.1±2.7	263.6±16.1	1581.0±4.3	112.6±6.9
	H016	900			1.27±0.08	3.10±0.27	1353.3±2.2	232.3±15.6	1583.4±1.9	112.0±2.7
	H101	280	1.62±0.15	0.97±0.11	0.73±0.06	1.57±0.19	1357.6±4.8	245.0±5.3	1597.7±1.8	91.6±11.9
	H102	400	1.52±0.21	0.34±0.10	0.69±0.03	1.87±0.12	1347.2±4.6	227.8±8.2	1598.1±1.4	70.8±4.9
Friction Exp.	HVR2957	40	1.82±0.25	1.12±0.43	0.73±0.04	1.49±0.14	1354.7±2.3	243.1±5.5	1599.4±1.9	83.8±8.1
	HVR2919	120	1.69±0.17	0.96±0.18	0.72±0.02	1.55±0.11	1352.5±1.8	241.5±4.2	1599.1±1.2	78.5±4.6
	HVR2956	250	1.57±0.22	0.84±0.26	0.70±0.02	1.60±0.12	1358.7±2.1	260.5±6.6	1598.9±0.9	80.5±3.9
Pristine Host Rock for Exp.			1.64±0.17	0.83±0.12	0.67±0.04	1.60±0.16	1353.2±4.6	246.6±5.5	1600.0±1.2	74.2±9.8

[a]Exp., experiment.

(average, 1599.03 ± 1.0 cm^{-1}). The Γ_G value in the PSZ sample (61.9 ± 6.8 cm^{-1}) was lower than the values for the black gouge samples and the surrounding deformed/host rocks (range, 70.9–105.3 cm^{-1}). Among the I_D/I_G ratios, and ω_D and ω_G values obtained by means of linear baseline compensation (supporting information Table S1), only the ω_D value had an anomaly for the PSZ sample: the value for the PSZ sample was 1343.6 ± 5.5 cm^{-1}, whereas the average value for the black gouge samples and the surrounding deformed/host rocks was 1357.5 ± 5.2 cm^{-1}.

3.3. IR Spectra of Products Obtained From Heating and Friction Experiments

We measured the IR absorption spectra of products obtained by subjecting carbonaceous materials to heating and friction experiments (Figure 5). IR absorption by a chemical species depends, in a strict sense, both on the concentration of the species and on the sample thickness (according to the Lambert-Beer law) and the thickness was roughly controlled in our measurements. In the spectra of the products obtained by heating at a rate of 10°C min^{-1} under Ar, the sharp absorbance peaks at 2960, 2930, and 2860 cm^{-1} became very weak at 400°C and disappeared at 700°C. The sharp absorbance peak at 1600 cm^{-1} became weak at 400°C and was almost completely gone at 700°C. The weak absorbance peak at 1050 cm^{-1} also became weak at 400°C and was almost completely gone at 700°C. The broad absorbance at around 3700–3000 cm^{-1} became weak at 100°C, was very weak at 400°C, and completely disappeared at 700°C. The weak absorbance peak at 1680 cm^{-1} disappeared at 700°C, but this peak in the spectra of the pristine host-rock sample and the sample heated to 100°C was very weak, which probably indicates large fluctuation of the initial concentration within the host-rock samples. The products obtained by heating at a rate of 10°C min^{-1} in air showed similar changes in their spectra relative to the spectra of the pristine sample. The absorbance peaks at 2960, 2930, 2860, and 1600 cm^{-1} seemed relatively weak compared with those in the spectra of products obtained under Ar. At 400°C, the products obtained by heating at a rate of 500°C min^{-1} under Ar showed more-intense peaks at 2960, 2930, and 2860 cm^{-1} than did the products obtained by heating at 10°C min^{-1}, but the changes in the peak at 1600 cm^{-1} were similar at the two heating rates. All the products obtained from the friction experiments in air retained the absorbance peaks at 2960, 2930, 2860, 1680, 1600, and 1050 cm^{-1}.

We determined CH_2/CH_3 and $CH_2/C{=}C$ peak ratios for the products from all the experiments and compared them with the corresponding ratios for the pristine host-rock samples (Table 3). For the products obtained by heating at 10°C min^{-1} under Ar, the CH_2/CH_3 ratios did not vary systematically from those of the pristine samples (no ratios are shown for temperatures of ≥700°C because the peaks were not present at those temperatures). The $CH_2/C{=}C$ ratios decreased with increasing temperature and reached zero at 700°C because the CH_2 peak disappeared. The products obtained by heating at 10°C min^{-1} in air showed ratios and temperature dependence similar to those observed in the experiments under Ar, but the $CH_2/C{=}C$ ratios at 100

and 300°C were approximately half of those for the Ar experiments at the same temperatures. In the experiment at a heating rate of 500°C min^{-1} under Ar, both ratios were similar to those in the experiment at 10°C min^{-1} under Ar. Neither ratio changed systematically in any of the products from the friction experiment.

3.4. Raman Spectra of Products Obtained From Heating and Friction Experiments

We measured the Raman spectra of products obtained by subjecting the carbonaceous materials to heating and friction experiments (Figure 5). In the products obtained from the experiment at a heating rate of 10°C min^{-1} under Ar, both the D and the G bands weakened with increasing temperature and were almost completely gone at 900°C. Small shoulder peaks at around 1150, 1280, 1450, and 1700 cm^{-1}, which were clearly observed in the pristine host-rock sample, disappeared at 500°C. The products obtained at a heating rate of 10°C min^{-1} in air showed spectral changes similar to the changes observed for the products obtained under Ar. The products obtained at 500°C min^{-1} under Ar showed almost no change relative to the pristine sample. Slight shoulder peaks were observed in the experiment with a target temperature of 400°C. None of the products from the friction experiments in air showed any discernible changes relative to the pristine sample.

We determined spectral parameters (I_D/I_G, A_D/A_G, ω_D, ω_G, Γ_D, and Γ_G) for the products from all the experiments and compared them to the parameters for the pristine host-rock sample (Table 3). In the products obtained at 10°C min^{-1} under Ar, the I_D/I_G ratios increased with increasing temperature beyond 500°C. The A_D/A_G ratios also increased with increasing temperature beyond 400°C. The ω_D, ω_G, and Γ_D values did not change relative to those of the pristine sample. The Γ_G values for the products obtained at 700 and 900°C (101.5 ± 6.8 and 113.9 ± 3.1 cm^{-1}, respectively) were higher than the value for the pristine sample (74.2 ± 9.8 cm^{-1}). The products obtained by heating at 10°C min^{-1} in air showed ratios and temperature dependence similar to those for the experiments under Ar. The parameters for the products obtained by heating at 500°C min^{-1} under Ar were virtually identical to those of the pristine sample. The products from the friction experiments also showed no specific changes relative to the pristine sample. In contrast, the I_D/I_G ratios determined by means of linear baseline compensation for experiments under Ar and in air at a heating rate of 10°C min^{-1} increased with increasing temperature beyond 700°C, but the ω_D and ω_G values determined in the same way showed no specific changes.

4. Discussion

4.1. Changes of IR and Raman Spectra With Increasing Temperature and Explanation of the Changes

First, we will briefly review the molecular structure of carbonaceous materials and how it changes with maturation. Carbonaceous materials within sedimentary rocks, such as kerogen, consist of an extremely heterogeneous cross-linked network of organic macromolecules [e.g., *Poutsma*, 1987; *Mathews and Chaffee*, 2012]. Lignite, the lowest rank of coal, consists of linked aromatic rings and cross-linked aliphatic side chains with a variety of functional groups such as alicyclic groups and carboxylic acid groups [e.g., *Wender*, 1976]. Thermal evolution during diagenesis is accompanied by the breaking of weak bonds, aromatization, and structural rearrangement [*Behar and Vandenbroucke*, 1987], and as a result, high-rank coals (bituminous and anthracite) consist of relatively large cross-linked pericondensed aromatic and alicyclic components [*Lazarov and Marinov*, 1987] that ultimately form large aromatic sheets and stack the sheets [*Nyathi et al.*, 2013]. However, the rapid heating under low-fugacity oxygen that occurs in a slip zone during earthquake slip can pyrolyze carbonaceous materials. Pyrolysis generally produces gaseous and liquid products and leaves a solid residue richer in carbon content than the original material. The volatile fraction consists of various hydrocarbons such as aromatic, aliphatic, and phenolic compounds with low molecular weights [e.g., *Pandolfo et al.*, 1988; *Lievens et al.*, 2013].

With this background information in mind, we evaluated the changes in the IR spectra with increasing temperature. The aliphatic CH_2 and CH_3 absorbance peaks at 2960 and 2930 cm^{-1}, respectively, became very weak at 400°C and disappeared at 700°C. Heating in air enhanced the weakening of the peaks at lower temperatures (100 and 300°C), and a rapid heating rate (500°C min^{-1}) delayed the weakening. The weakening at 400°C was due to thermal breakage of chemical bonds in aliphatic chains; these thermal reactions include side group reactions and chain scission reactions [e.g., *Xu et al.*, 2014], as evidenced by the presence of aliphatic components such as 1-decanol and 1-pentadecene in the pyrolysates produced by heating pristine host-rock carbonaceous materials at 400°C (Figure 2a). The first endothermic weight loss in the 200–

400°C temperature range observed by TG-DSC (Figure 2c) is consistent with this thermal breakage. This reaction was affected by kinetics and atmospheric conditions. In contrast, the aromatic C=C and C–H absorbance peaks at 1600 and 1050 cm^{-1} became weak at 400°C and disappeared almost completely at 700°C. Heating in air resulted in weakening at lower temperatures (100 and 300°C), but there was no discernible difference between the fast and slow heating rates (500 and 10°C min^{-1}, respectively). The broad absorbance peak at around 3400 cm^{-1} started to decrease at 100°C, owing to release of absorbed H_2O molecules from the sample surface. The peak decreased even more at 400°C, which is consistent with the decrease in the 1600 cm^{-1} absorbance peak. It is therefore conceivable that these decreases with increasing temperature at 400°C reflect the loss of phenolic OH, clearly evidenced by the detection of phenols in the pyrolysates of carbonaceous materials heated at 400°C (Figure 2a). The release of phenols during pyrolysis is a typical feature of lignin and low-rank coal [e.g., *Hatcher*, 1990; *Dorrestijn et al*., 2000; *Collard and Blin*, 2014]. This reaction in our experiments might not have been markedly affected by kinetics and atmospheric conditions. The carbonyl C=O stretch absorbance peak at 1680 cm^{-1} disappeared at 700°C, probably as a result of breaking of the bond between carbonyl groups and the parent compound, but the initial concentrations of carbonyl group within the pristine host-rock samples might not be homogeneous.

The heating experiments resulted in the weakening of the D and G bands in the Raman spectra with increasing temperature (the bands almost completely disappeared at 900°C) and the disappearance of the shoulder peaks at 500°C. Because benzene has high thermal stability and is not decomposed below 900°C [e.g., *Zanetti and Egloff*, 1917] and because graphene is stable even at 2300°C [e.g., *Kim et al*., 2010], the Raman intensity due to the graphitic crystallite structure should not be weakened at temperatures of $<$900°C. As mentioned above, *Li et al*. [2006] attributed the G and D bands in highly disordered carbonaceous materials to the aromatic quadrant ring-breathing mode and to the disorder of aromatic rings, respectively, and reported that the intensities of these bands in the spectra of the solid residue decreased with increasing temperature. Taken together, these results suggest that our carbonaceous materials consist of small amounts of graphitic components and are probably composed mainly of aromatic rings with various functional groups that undergo pyrolysis. Large amounts of aromatic compounds such as benzofuran, 1-naphthol, and anthracenedione were detected in the pyrolysates from pristine host-rock's carbonaceous materials heated to 700°C (Figure 2b), and the volatile fraction reached 48 wt % (Figure 2c), so the weakening of the D and G band intensities with increasing temperature may have been due to the thermal decomposition of aromatic rings and other functional groups during pyrolysis. In addition, the disappearance of the shoulder peaks, attributed to vibrations of aliphatic cyclic components and carbonyl groups, may also have resulted from the thermal decomposition as well as the decreases and disappearances of most of the functional groups in the IR spectra.

4.2. Comparisons of IR and Raman Spectra of Samples From the Chelungpu Fault With Those of Products From Heating and Friction Experiments

The IR and Raman spectra of the PSZ sample showed very weak aliphatic CH_2 and CH_3 absorbance peaks, no C=O absorbance peak, a very weak C=C absorbance peak, a very weak bump at around 3400 cm^{-1}, very weak G and D bands, and no shoulder peaks. The results from the heating and friction experiments suggest that these peaks correspond to high temperatures of $\geq$400, $\geq$700, $\geq$400, $\geq$400, $\geq$700, and $\geq$500°C, respectively. It is therefore conceivable that the frictional heat in the PSZ reached 700°C.

Changes of the CH_2/CH_3, CH_2/C=C, I_D/I_G, and A_D/A_G ratios in the experimentally obtained products with increasing temperature are shown in Figure 6, along with the corresponding values for the PSZ sample, the host-rock samples, and the pristine samples used in the experiments. The CH_2/CH_3 ratios in the experimental products were almost constant, had large standard deviations, and were inconsistent with the reported trend that the ratios decreased at high temperature [*Huang and Otten*, 1998; *Kebukawa et al*., 2010]. The CH_2/C=C ratios in the experimental products decreased with increasing temperature, and this trend agrees well with the presence of immature kerogen in middle Holocene peat strata [*Zeng and Wu*, 2007]. However, the experiments did not reproduce the ratio for the PSZ sample. This disagreement may have been the result of inaccurate calculations due to the weakness of the absorbance peaks. In contrast, the I_D/I_G and A_D/A_G ratios increased with increasing temperature and crossed the corresponding values of the PSZ sample at 500–600 and 500–700°C, respectively. However, the I_D/I_G ratios for the PSZ and host-rock samples were closer than were the A_D/A_G ratios for the two samples, so the latter might be more representative of the actual temperature reached in the fault.

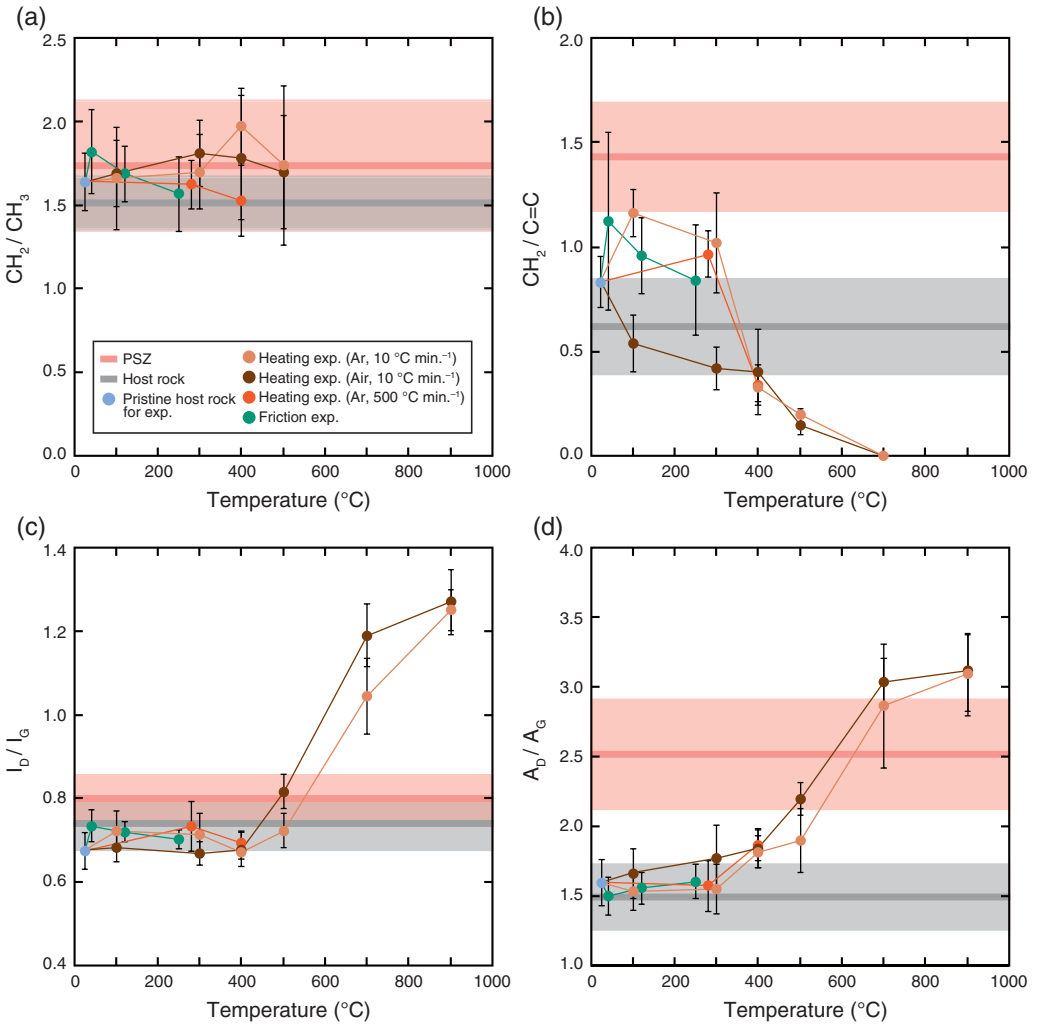

Figure 6. Temperature dependences of IR and Raman spectral parameters: (a) CH_2/CH_3 ratios in the IR spectra, (b) $CH_2/C{=}C$ ratios in the IR spectra, (c) I_D/I_G ratios in the Raman spectra, and (d) A_D/A_G ratios in the Raman spectra. PSZ, primary slip zone and exp., experiment.

Taking these changes of IR and Raman spectra and A_D/A_G ratios with increasing temperature into account, we concluded that the PSZ reach a high temperature of approximately 700°C. However, in the strict sense, this temperature determination includes an uncertainty of roughly ±100°C stemming from the 200°C temperature step of our heating experiments at >500°C. In addition, kinetics could affect the progress of the reactions leading to the changes, which was confirmed by our results for heating experiments conducted at rates of 10 and 500°C min^{-1}. The faster heating rate delayed the reactions, and such a delay might also have occurred during earthquake slip because of the ultrafast heating rate (several hundreds of degrees Celsius per second). Thus, the actual temperature reached in the fault might have been somewhat higher than 700°C, but we cannot be certain owing to the lack of kinetic parameters. Atmospheric conditions also affect the progress of the reactions, and the presence of air can lead to different types of reactions such as oxidation. But air atmosphere is unlikely to have existed in the deep environment, at low oxygen fugacity. No influence of shear deformation was observed in the IR or Raman spectra, but the temperatures attained were not high in the friction experiments (≤250°C).

4.3. Correlations Between Raman Spectral Parameters and Temperature

The I_D/I_G and A_D/A_G ratios of carbonaceous materials not only are correlated with metamorphic grade [e.g., *Jehlicka and Beny*, 1992; *Wopenka and Pasteris*, 1993] but also have been used as geothermometers [*Beyssac et al.*, 2002; *Rahl et al.*, 2005; *Lahfid et al.*, 2010; *Kouketsu et al.*, 2014]. *Morga* [2011] reported that the I_D/I_G ratio and the ratio of A_D to the total area of all the Raman bands (including the G band) of inertinite from

the Upper Silesian Coal Basin of Poland increased when heated to temperatures of ≥800°C at a rate of 60°C min^{-1} under Ar and that the ratios did not change systematically at ≤600°C. *Huang et al.* [2010] also reported no systematic change in the I_D/I_G ratio of kerogen from the Gutingkeng mudstone in southern Taiwan with increasing temperature at temperatures of ≤600°C, as indicated by in situ measurement during heating at a rate of 25°C min^{-1} under Ar. However, *Zickler et al.* [2006] demonstrated that the I_D/I_G ratio of spruce wood increases at temperatures of ≥500°C during heating at a rate of 2°C min^{-1} under nitrogen, and these investigators found that the in-plane size of the graphitic crystallites, determined from X-ray diffraction data and the Scherrer equation, increases with increasing temperature. *Li et al.* [2006] also reported that in brown coal, the I_D/I_G ratio increases with increasing temperature from 500 to 700°C and that the ratio of A_D to the total area of all the bands (including the G band) increases from 500 to 900°C; these increases were considered to result from aromatization. Thus, low-rank kerogen may generally show an increase in I_D/I_G ratio with increasing temperature. In contrast, *Beyssac et al.* [2002] and *Rahl et al.* [2005], using I_D/I_G as a geothermometer, showed inverse correlation between the ratio of A_D to the total area of all the bands (including the G band) and temperature, which could have resulted from a decrease in the in-plane crystalline size of the hexagonal plane of graphene layers. Rapid heating during earthquake slip may promote a reaction in carbonaceous materials that is different from the reactions involved in long-term metamorphism.

The increases in I_D/I_G and A_D/A_G at temperatures of ≥400 and ≥500°C, respectively, in our carbonaceous materials seem to have resulted from the growth of aromatic rings and the dehydrogenation of alicyclic hydrocarbons. This condensation process was evidenced by the exothermic shift in the DSC curve at temperatures of ≥400°C and the exotherms at ≥570°C with a broad peak at around 770°C and a slight weight loss (Figure 2c); we consider these changes at high temperature to have resulted from contraction reactions such as formation of stronger C–C bonds and dehydrogenation [e.g., *Strezov et al.*, 2000]. The sharp endothermic peak at 530°C without a large weight loss might have been due to thermal decomposition of inorganic sulfur compounds, as indicated by the detection of sulfur dioxide and carbon disulfide in the pyrolysates obtained upon heating at 700°C. However, we cannot assign this peak with certainty at this time. In the PSZ sample, the presence of small amounts of aromatic ester, as indicated by the IR absorbance peaks at 1730 and 1250 cm^{-1}, may have been due to condensation reactions between carboxylic acids and phenols.

The effect of temperature on the relationships between Γ_D and ω_D and between Γ_G and ω_G for the various experiments are shown in Figures 7a and 7b. The values of ω_D decreased with decreasing Γ_D, and the PSZ sample had the lowest ω_D and Γ_D values. However, none of the experiments showed systematic changes or reproduced the values observed for the PSZ sample. The products obtained at higher temperatures showed higher Γ_G and lower ω_G values than the products obtained at lower temperatures; the values were similar to those observed for coal samples from the Penn State Coal Bank [*Guedes et al.*, 2010].

Correlations between Raman spectral parameters and vitrinite reflectance sometimes provide information about the maturity of kerogens and coals [e.g., *Kelemen and Fang*, 2001; *Guedes et al.*, 2010, 2012; *Zhou et al.*, 2014]. For reference, we show the relationships between I_D/I_G and vitrinite reflectance (R_o, reported by *Maekawa et al.* [2014]), between A_D/A_G ratio and R_o, and between Γ_G and R_o in the PSZ and surrounding deformed/host rocks in Figures 7c–7e. The I_D/I_G ratios did not show good correlation with R_o; similar results were reported for low-maturity bitumen ($R_o < 1.5$) from the Permian strata of the Changjianggou area of southwestern China [*Zhou et al.*, 2014]. However, A_D/A_G was linearly related to R_o with ($R = 0.79$) and Γ_G was negatively correlated with R_o ($R = 0.62$). Similar correlations have been reported for bitumen heated in an autoclave under vacuum [*Zhou et al.*, 2014] and for natural coal from the Penn State Coal Bank [*Guedes et al.*, 2010]. Thus, these Raman parameters together with vitrinite reflectance could be proxies for maturity assessment. None of the other spectral parameters (Γ_D, ω_D, and ω_G) were correlated with R_o (supporting information Figure S2).

4.4. Estimations of Shear Stress and Frictional Coefficient in the Slip Zone During the Chi-Chi Earthquake

The change in temperature in the slip zone can be expressed by a one-dimensional heat and thermal diffusion equation:

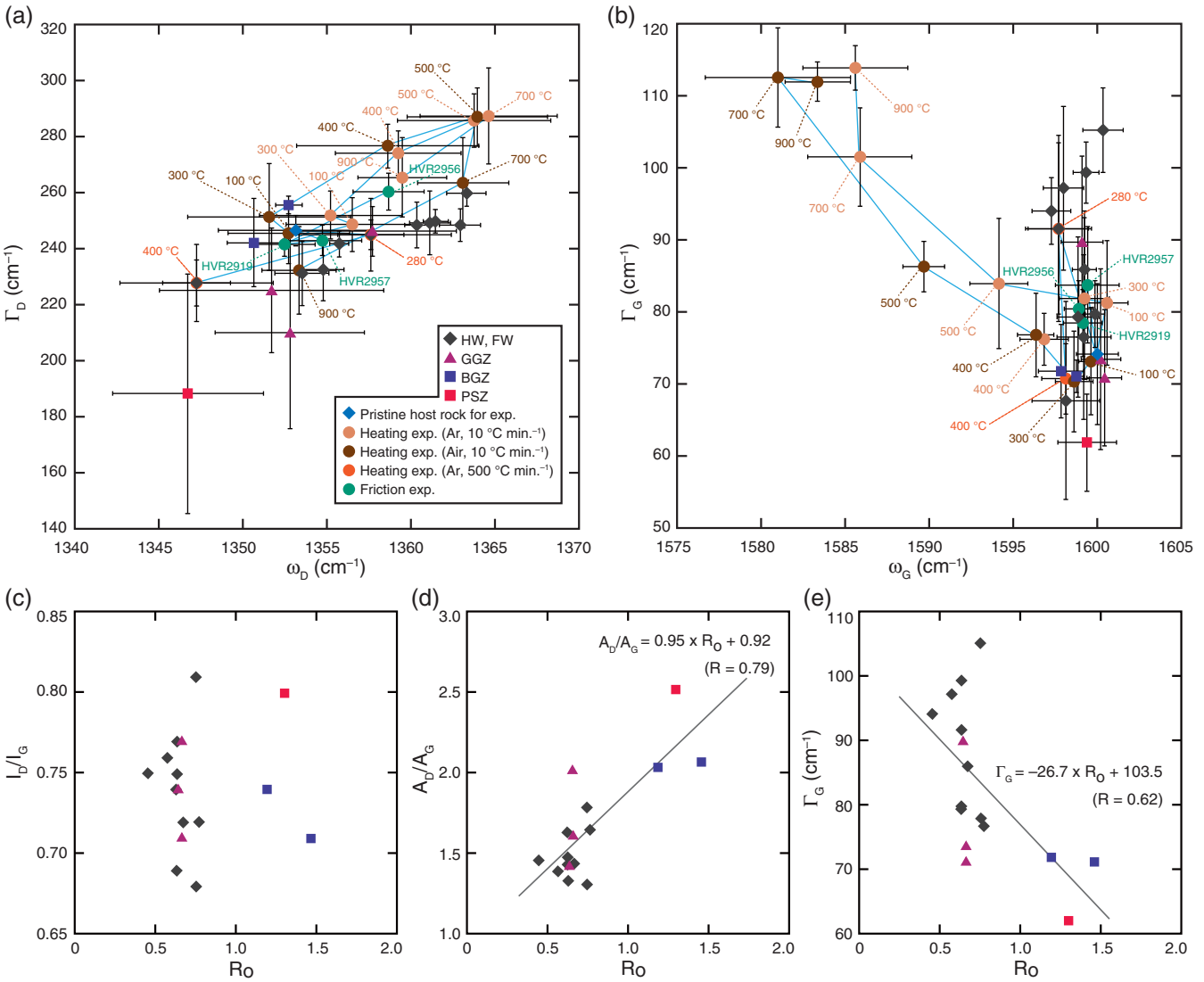

Figure 7. Relationships between Raman spectral parameters and between Raman spectral parameters and vitrinite reflectance (R_o). (a, b) Relationships between D and G band parameters, respectively. Γ, peak position; ω, band width. Data for all the samples from the Chelungpu fault and surrounding rocks and from the heating and friction experiments are plotted. (c) I_D/I_G versus R_o. (d) A_D/A_G versus R_o. R, correlation coefficient. (e) Γ_G versus R_o.

$$\frac{\partial T}{\partial t}-\frac{\partial}{\partial x}\left(\kappa(T)\frac{\partial T}{\partial x}\right)-\frac{\partial}{\partial t}\left(\frac{\tau D}{wC_p\rho}\right)=0 \quad (1)$$

where T is a temperature, t is a time, $\kappa(T)$ is a thermal diffusivity as a function of temperature, x is the distance from the center of the slip zone ($x = 0$), τ is a shear stress, D is a slip distance, w is a slip-zone thickness, C_p is a specific heat capacity, and ρ is a density. For simplicity, convective heat transfer, endothermic processes, and dynamic fault weakening are ignored. For $T < 573$°C, $\kappa = 2.27 \times 10^{-4}\, T^{-1} + 1.78 \times 10^{-7}$ m^2 s^{-1} (where T is in Kelvin); and for $T \geq 573$°C, $\kappa = 4.73 \times 10^{-7}$ m^2 s^{-1}. The C_p value of Chinshui shale, which is the host rock of the Chelungpu fault, has been determined to be approximately 1300 J kg^{-1} K^{-1} [*Hirono and Hamada*, 2010]. In the Chi-Chi earthquake PSZ, $w = 5$ mm [*Chou et al.*, 2012], $\rho = 2200$ kg m^{-3} [*Hirono et al.*, 2006], the rise time was 6 s, and the total slip distance was 8.3 m [*Ma et al.*, 2006]. The initial temperature before the earthquake was measured to be 46.5°C [*Kano et al.*, 2006]. By solving equation (1) with the estimated temperature of $T = 700$°C under a 0.01 s time increment, a 0.5 mm grid size, and the boundary condition of $T = 46.5$°C at $x > 200$ mm, the value of τ was determined to be 1.13 MPa. For $T = 600$ and 800°C that obtained from the upper and lower bounds obtained from the uncertainty of the IR and Raman spectroscopic evaluations, the corresponding values of τ were 0.95 and 1.30 MPa, respectively. Heat

conducted from the PSZ could not affect the infrared and Raman spectra of carbonaceous materials from the surrounding samples: for positions 40 mm away from the PSZ, the highest temperatures experienced were calculated to be 95, 104, and 114°C for PSZ temperatures of 600, 700, and 800°C, respectively (supporting information Figure S3). In fact, the adjacent gray gouge sample at 1136.39 m had IR absorbance peaks for aliphatic CH_2 and CH_3, C=O, and C=C and Raman G and D bands with shoulder peaks that correlated to <400°C, and this sample showed no specific anomaly in other temperature proxies: concentrations of fluid-mobile trace elements, Sr isotope ratio, and magnetic minerals that correlated to at least <350°C [*Ishikawa et al*., 2008; *Mishima et al*., 2009; *Chou et al*., 2012].

Next, we calculated the friction coefficient from the τ value in the PSZ associated with the Chi-Chi earthquake. The effective vertical stress around sample FZB1136 was 17.8 MPa (rock density, 2600 kg m^{-3}), under the assumptions of hydrostatic pore-fluid pressures and a fault plane dip of 35° [*Hirono et al*., 2007a]. Assuming that the stress normal to the fault (σ_n) was equal to the stress in the static state and that the horizontal stress (σ_H) was equal to the vertical stress (σ_V), the stress normal to the fault was 17.8 MPa, which gives an apparent friction coefficient of 0.06. For a thrust fault, the maximum σ_H is higher than σ_V [*Sibson*, 1974]. Assuming that σ_n is equal to the static stress state and that maximum σ_H is two times σ_V, then σ_n is 43.7 MPa, which gives an apparent friction coefficient of 0.03. Regardless of the uncertainty of the inferred τ values (0.95–1.30 MPa), the apparent friction coefficient ranged from 0.02 to 0.07.

This low friction coefficient range (0.02–0.07) agrees well with the seismological observations of low levels of high-frequency radiation, fast slip velocities, and high slip displacement, all of which indicate a low level of friction on the fault [*Ma et al*., 2003]. The coefficient range is also consistent with the residual heat anomaly of 0.06°C, which corresponds to an apparent friction coefficient of 0.04–0.08, obtained by borehole temperature measurement in Hole A of the Taiwan Chelungpu-Fault Drilling Project [*Kano et al*., 2006].

The low friction coefficient may have resulted from dynamic weakening of the fault strength (shear resistance). *Tanikawa et al*. [2009] experimentally evaluated the hydraulic properties in and around the slip zone within the Chelungpu fault and confirmed that the properties have the potential to trigger thermal pressurization, as indicated by numerical analyses of fault slip. In addition, anomalous concentrations of fluid-mobile elements and Sr isotope ratios resulting from the interaction of minerals with high-temperature (≥350°C) fluids have been reported [*Ishikawa et al*., 2008]. Therefore, the low friction calculated from the results of our study and from the borehole temperature measurements of *Kano et al*. [2006] suggest that thermal pressurization occurred along the Chelungpu fault during the Chi-Chi earthquake.

5. Conclusions

Herein, we have described the use of IR and Raman spectroscopies of carbonaceous materials to determine the record of frictional heating in the Chelungpu fault. The IR absorbance peaks of various functional groups such as aliphatic CH, aromatic C=C, and phenolic OH, as well as I_D/I_G and A_D/A_G ratios obtained from the Raman spectra, were used to estimate the temperature reached in the fault. In the IR spectra of carbonaceous materials extracted from the PSZ sample, we observed the disappearance or weakening of the peaks for these functional groups, as well as weakening of the D and G bands in the Raman spectra and high I_D/I_G and A_D/A_G ratios; these changes resulted from decomposition and condensation reactions during pyrolysis at high temperature (~700 ± 100°C). However, the temperature dependence of these changes was complex and probably depends on the initial molecular structure of the materials, which is related to degree of maturation; therefore, a complete understanding of the temperature dependence will require multiple approaches involving not only IR and Raman spectroscopies but also pyrolysis GC/MS and TG-DSC. In addition, other phenomena, not assessed in our study, may be involved in the changes in the carbonaceous materials. For example, shear deformation could facilitate the flattening of existing pore spaces and mechanical rotation of stacks of aromatic layers, leading to the formation of graphite [*Ross et al*., 1991; *Bustin et al*., 1995], although graphitization was not detected in our friction experiment, probably because the temperature (250°C) was too low to lead to changes in the IR and Raman spectra. Release of H_2O and CO_2 from coexisting clay minerals and carbonate minerals (referred to as hydrous pyrolysis) [e.g., *Castelli et al*., 1990] may have affected the pyrolysis of the carbonaceous materials, and the release of metal cations from coexisting minerals also affects the progress of pyrolysis [e.g., *Karabakan and Yurum*, 1998]. Environmental pressure conditions can shift the peak positions of the D and G bands in the Raman spectrum [*Zeng and*

Wu, 2007; *Huang et al*., 2010]. Therefore, further analysis of various types of carbonaceous materials from various types of fault rocks, in combination with laboratory heating and friction experiments, is required before a universal proxy for detecting heat signatures along faults can be developed.

Acknowledgments
We thank Hideki Mukoyoshi, Wataru Tanikawa, and Shunya Kaneki for technical support for our friction experiment and thermal modeling. We also thank Associate Editor Wendy Panero and Editor Yusuke Yokoyama for their constructive suggestion. This research was supported by a Grant-in-Aid for Young Scientists (A) from the Japan Ministry of Education, Science, Sports, and Culture (23684039, 2013).

References

Alexander, C. M. O. D., M. Fogel, H. Yabuta, and G. D. Cody (2007), The origin and evolution of chondrites recorded in the elemental and isotopic compositions of their macromolecular organic matter, *Geochim. Cosmochim. Acta*, *71*, 4380–4403.
Behar, F., and M. Vandenbroucke (1987), Chemical modelling of kerogens, *Org. Geochem.*, *11*, 15–24.
Bent, R., and J. K. Brown (1961), The infra-red spectra of macerals, *Fuel*, *40*, 47–56.
Beyssac, O., B. Goffe, C. Chopin, and J. N. Rouzaud (2002), Raman spectra of carbonaceous material in metasediments: A new geothermometer, *J. Metamorph. Geol.*, *20*, 858–871.
Bonal, L., E. Quirico, M. Bourot-Denise, and G. Montagnac (2006), Determination of the petrologic type of CV3 chondrites by Raman spectroscopy of included organic matter, *Geochim. Cosmochim. Acta*, *70*, 1849–1863.
Busemann, H., C. M. O. Alexander, and L. R. Nittler (2007), Characterization of insoluble organic matter in primitive meteorites by micro Raman spectroscopy, *Meteorit. Planet. Sci.*, *42*, 1387–1416.
Bustin, R. M. (1983), Heating during thrust faulting in the Rocky Mountains: Friction or fiction? *Tectonophysics*, *95*, 309–328.
Bustin, R. M., J. V. Ross, and J. N. Rouzaud (1995), Mechanisms of graphite formation from kerogen: Experimental evidence, *Int. J. Coal Geol.*, *28*, l–36.
Castelli, A., M. A. Chiaramonte, P. L. Beltrame, and P. Carniti (1990), Thermal degradation of kerogen by hydrous pyrolysis: A kinetic study, *Org. Geochem.*, *16*, 75–82.
Chen, K. C., B. S. Huang, J. H. Wang, W. G. Huang, T. M. Chang, R. D. Hwang, H. C. Chiu, and C. P. Tsai (2001), An observation of rupture pulses of the 20 September 1999 Chi-Chi, Taiwan, earthquake from near-field seismograms, *Bull. Seismol. Soc. Am.*, *91*, 1247–1254.
Chou, Y. M., S. S. Song, C. Aubourg, T. Q. Lee, A. M. Boullier, Y. F. Song, E. C. Yeh, L. W. Kuo, and C. Y. Wang (2012), An earthquake slip zone is a magnetic recorder, *Geology*, *40*, 551–554.
Cody, G. D., and C. M. O. D. Alexander (2005), NMR studies of chemical structural variation of insoluble organic matter from different carbonaceous chondrite groups, *Geochim. Cosmochim. Acta*, *69*, 1085–1097.
Cody, G. D., C. M. O. D. Alexander, and F. Tera (2002), Solid-state (^{1}H and ^{13}C) nuclear magnetic resonance spectroscopy of insoluble organic residue in the Murchison meteorite: A self-consistent quantitative analysis, *Geochim. Cosmochim. Acta*, *66*, 1851–1865.
Collard, F. X., and J. Blin (2014), A review on pyrolysis of biomass constituents: Mechanisms and composition of the products obtained from the conversion of cellulose, hemicelluloses and lignin, *Renew. Sustain. Energy Rev.*, *38*, 594–608.
Cuesta, A., P. Dhamelincourt, J. Laureyns, A. Martinez-Alonso, and J. M. D. Tascon (1998), Comparative performance of X-ray diffraction and Raman microprobe techniques for the study of carbon materials, *J. Mater. Chem.*, *8*, 2875–2879.
Czuchajowski, L. (1961), Infra-red spectra of carbonized coals and coal-like materials and some absorption changes during subsequent oxidation, *Fuel*, *40*, 361–374.
Dorrestijn, E., L. J. J. Laarhoven, I. W. C. E. Arends, and P. Mulder (2000), The occurrence and reactivity of phenoxyl linkages in lignin and low rank coal, *J. Anal. Appl. Pyrolysis*, *54*, 153–192.
Flynn, G. J., L. P. Keller, M. Feser, S. Wirick, and C. Jacobsen (2003), The origin of organic matter in the solar system: Evidence from the interplanetary dust particles, *Geochim. Cosmochim. Acta*, *67*, 4791–4806.
Friedel, R. A., and G. L. Carlson (1972), Difficult carbonaceous materials and their infra-red and Raman spectra: Reassignments for coal spectra, *Fuel*, *51*, 194–198.
Green, P. D., C. A. Johnson, and K. M. Thomas (1983), Applications of laser Raman microprobe spectroscopy to the characterization of coals and cokes, *Fuel*, *62*, 1013–1023.
Guedes, A., B. Valentim, A. C. Prieto, S. Rodrigues, and F. Noronha (2010), Micro-Raman spectroscopy of collotelinite, fusinite and macrinite, *Int. J. Coal Geol.*, *83*, 415–422.
Guedes, A., B. Valentim, A. C. Prieto, and F. Noronha (2012), Raman spectroscopy of coal macerals and fluidized bed char morphotypes, *Fuel*, *97*, 443–449.
Guo, Y., and R. M. Bustin (1998), FTIR spectroscopy and reflectance of modern charcoals and fungal decayed woods: Implications for studies of inertinite in coals, *Int. J. Coal Geol.*, *37*, 29–53.
Hatcher, P. G. (1990), Chemical structural models for coalified wood (vitrinite) in low rank coal, *Org. Geochem.*, *16*, 959–968.
Hayatsu, R., S. Matsuoka, E. Anders, R. G. Scott, and M. H. Studier (1977), Origin of organic matter in the early solar system—VII. The organic polymer in carbonaceous chondrites, *Geochim. Cosmochim. Acta*, *41*, 1325–1339.
Hirono, T., and Y. Hamada (2010), Specific heat capacity and thermal diffusivity and their temperature dependencies in a rock sample from adjacent to the Taiwan Chelungpu fault, *J. Geophys. Res.*, *115*, B05313, doi:10.1029/2009JB006816.
Hirono, T., et al. (2006), High magnetic susceptibility of fault gouge within Taiwan Chelungpu fault: Nondestructive continuous measurements of physical and chemical properties in fault rocks recovered from Hole B, TCDP, *Geophys. Res. Lett.*, *33*, L15303, doi:10.1029/2006GL026133.
Hirono, T., et al. (2007a), Nondestructive continuous physical property measurements of core samples recovered from Hole B, Taiwan Chelungpu-fault Drilling Project, *J. Geophys. Res.*, *112*, B07404, doi:10.1029/2006JB004738.
Hirono, T., et al. (2007b), A chemical kinetic approach to estimate dynamic shear stress during the 1999 Taiwan Chi-Chi earthquake, *Geophys. Res. Lett.*, *34*, L19308, doi:10.1029/2007GL030743 (Correction, Geophys. Res. Lett., 35, doi:10.1029/2007GL032512, 2008).
Hirono, T., et al. (2008), Characterization of slip zone associated with the 1999 Taiwan Chi-Chi earthquake: X-ray CT image analyses and microstructural observations of the Taiwan Chelungpu fault, *Tectonophysics*, *449*, 63–84.
Hirono, T., K. Ujiie, T. Ishikawa, T. Mishima, Y. Hamada, M. Tanimizu, W. Soh, and M. Kinoshita (2009), Estimation of temperature rise in a shallow slip zone of the megasplay fault in the Nankai Trough, *Tectonophysics*, *478*, 215–220.
Hirono, T., T. Ishikawa, H. Masumoto, J. Kameda, H. Yabuta, and H. Mukoyoshi (2014), Re-evaluation of frictional heat recorded in the dark gouge of the shallow part of a megasplay fault at the Nankai Trough, *Tectonophysics*, *626*, 157–169.
Huang, E. P., E. Huang, S. C. Yu, Y. H. Chen, J. S. Lee, and J. N. Fang (2010), In situ Raman spectroscopy on kerogen at high temperatures and high pressures, *Phys. Chem. Miner.*, *37*, 593–600.
Huang, W. L., and G. A. Otten (1998), Oil generation kinetics determined by DAC-FS/IR pyrolysis: Technique development and preliminary results, *Org. Geochem.*, *5–7*, 1119–1137.

Ibarra, J. V., E. Munoz, and R. Moliner (1996), FTIR study of the evolution of coal structure during the coalification process, *Org. Geochem.*, *6–7*, 725–735.
Ikehara, M., et al. (2007), Low total and inorganic carbon contents within the Chelungpu fault, *Geochem. J.*, *41*, 391–396.
Ishikawa, T., et al. (2008), Coseismic fluid-rock interactions at high temperatures in the Chelungpu fault, *Nat. Geosci.*, *1*, 679–683.
Jehlicka, J., and C. Beny (1992), Application of Raman microspectrometry in the study of structural changes in Precambrian kerogens during regional metamorphism, *Org. Geochem.*, *18*, 211–213.
Johnson, C. A., J. W. Patrick, and K. M. Thomas (1986), Characterization of coal chars by Raman spectroscopy, X-ray diffraction and reflectance measurements, *Fuel*, *65*, 1285–1290.
Kano, Y., J. Mori, R. Fujio, H. Ito, T. Yanagidani, S. Nakao, and K. Ma (2006), Heat signature on the Chelungpu fault associated with the 1999 Chi-Chi, Taiwan earthquake, *Geophys. Res. Lett.*, *33*, L14306, doi:10.1029/2006GL026733.
Karabakan, A., and Y. Yurum (1998), Effect of the mineral matrix in the reactions of oil shale: 1. Pyrolysis reactions of Turkish Goynuk and US Green River Oil Shales, *Fuel*, *77*, 1303–1309.
Kebukawa, Y., S. Nakashima, and M. E. Zolensky (2010), Kinetics of organic matter degradation in the Murchison meteorite for the evaluation of parent-body temperature history, *Meteorit. Planet. Sci.*, *45*, 99–113.
Kelemen, S. R., and H. L. Fang (2001), Maturity trends in Raman spectra from kerogen and coal, *Energy Fuels*, *15*, 653–658.
Kim, K., W. Regan, B. Geng, B. Aleman, B. M. Kessler, F. Wang, M. F. Crommie, and A. Zettl (2010), High-temperature stability of suspended single-layer graphene, *Phys. Status Solidi RRL*, *4*, 302–304.
Kitamura, M., H. Mukoyoshi, P. M. Fulton, and T. Hirose (2012), Coal maturation by frictional heat during rapid fault slip, *Geophys. Res. Lett.*, *39*, L16302, doi:10.1029/2012GL052316.
Kouketsu, Y., T. Mizukami, H. Mori, S. Endo, M. Aoya, H. Hara, D. Nakamura, and S. Wallis (2014), A new approach to develop the Raman carbonaceous material geothermometer for low-grade metamorphism using peak width, *Isl. Arc*, *23*, 33–50.
Kuo, L. W., S. R. Song, E. C. Yeh, and H. F. Chen (2009), Clay mineral anomalies in the fault zone of the Chelungpu Fault, Taiwan, and their implications, *Geophys. Res. Lett.*, *36*, L18306, doi:10.1029/2009GL039269.
Kuo, L. W., S. R. Song, L. Huang, E. C. Yeh, and H. F. Chen (2011), Temperature estimates of coseismic heating in clay-rich fault gouges, the Chelungpu fault zone, Taiwan, *Tectonophysics*, *502*, 315–327.
Lahfid, A., O. Beyssac, E. Deville, F. Negro, C. Chopin, and B. Goffe (2010), Evolution of the Raman spectrum of carbonaceous material in low-grade metasediments of the Glarus Alps (Switzerland), *Terra Nova*, *22*, 354–360.
Landais, P., and A. Rochdi (1990), Reliability of semiquantitative data extracted from transmission microscopy-Fourier transform infrared spectra of coal, *Energy Fuels*, *4*, 290–295.
Lazarov, L., and S. P. Marinov (1987), Modelling the structure of a coking coal, *Fuel Process. Technol.*, *15*, 411–422.
Lee, Y. H., M. L. Hsieh, S. D. Lu, T. S. Shih, W. Y. Wu, Y. Sugiyama, T. Azuma, and Y. Kariya (2003), Slip vectors of the surface rupture of the 1999 Chi-Chi earthquake, western Taiwan, *J. Struct. Geol.*, *25*, 1917–1931.
Li, X., J. Hayashi, and C. Z. Li (2006), FT-Raman spectroscopic study of the evolution of char structure during the pyrolysis of a Victorian brown coal, *Fuel*, *85*, 1700–1707.
Lievens, C., D. Ci, Y. Bai, L. Ma, R. Zhang, J. Y. Chen, Q. Gai, Y. Long, and X. Guo (2013), A study of slow pyrolysis of one low rank coal via pyrolysis-GC/MS, *Fuel Process. Technol.*, *116*, 85–93.
Lin, R., and G. P. Ritz (1993), Studying individual macerals using IR microspectroscopy and implications on oil versus gas/condensate proneness and "low-rank" generation, *Org. Geochem.*, *20*, 695–706.
Lin, W., E.-C. Yeh, H. Ito, J.-H. Hung, T. Hirono, W. Soh, K.-F. Ma, M. Kinoshita, C.-Y. Wang, and S.-R. Song (2007), Current stress state and principal stress rotations in the vicinity of the Chelungpu fault induced by the 1999 Chi-Chi, Taiwan, earthquake, *Geophys. Res. Lett.*, *34*, L16307, doi:10.1029/2007GL030515.
Lin-Vien, D., N. B. Colthup, W. G. Fateley, and J. G. Grasselli (1991), *The Handbook of Infrared and Raman Characteristic Frequencies of Organic Molecules*, 497 pp., Academic, San Diego, Calif.
Ma, K. F., C. T. Lee, Y. B. Tsai, T. C. Shin, and J. Mori (1999), The Chi-Chi Taiwan earthquake: Large surface displacements on inland thrust fault, *Eos Trans. AGU*, *80*, 605–611.
Ma, K. F., T. R. Song, S. J. Lee, and S. I. Wu (2000), Spatial slip distribution of the September 20, 1999, Chi-Chi Taiwan earthquake: Inverted from teleseismic data, *Geophys. Res. Lett.*, *27*, 3417–3420.
Ma, K. F., E. E. Brodsky, J. Mori, T. R. Song, and H. Kanamori (2003), Evidence for fault lubrication during the 1999 Chi-Chi, Taiwan, earthquake (Mw7.6), *Geophys. Res. Lett.*, *30*(5), 1244, doi:10.1029/2002GL015380.
Ma, K., et al. (2006), Slip zone and energetics of a large earthquake from the Taiwan Chelungpu-fault Drilling Project, *Nature*, *444*, 473–476.
Maekawa, Y., T. Hirono, H. Yabuta, H. Mukoyoshi, M. Kitamura, M. Ikehara, W. Tanikawa, and T. Ishikawa (2014), Estimation of slip parameters associated with frictional heating during the 1999 Taiwan Chi-Chi earthquake by vitrinite reflectance geothermometry, *Earth Planets Space*, *66*, 28.
Martin, C. M., Q. Cai, S. Guha, W. Graupner, M. Chandrasekhar, and H. R. Chandrasekhar (2004), Raman modes in oligophenyls under hydrostatic pressure, *Phys. Status Solidi B*, *241*, 3339–3344.
Mastalerz, M., and R. M. Bustin (1993), Electron microprobe and micro-FTIR analyses, applied to maceral chemistry, *Int. J. Coal Geol.*, *24*, 333–345.
Mastalerz, M., and R. M. Bustin (1996), Application of reflectance micro-Fourier Transform infrared analysis to the study of coal macerals: An example from the Late Jurassic to Early Cretaceous coals of the Mist Mountain Formation, *Int. J. Coal Geol.*, *32*, 55–67.
Mathews, J. P., and A. L. Chaffee (2012), The molecular representations of coal—A review, *Fuel*, *96*, 1–14.
Matrajt, G., J. Borg, P. I. Raynal, Z. Djouadi, L. d'Hendecourt, G. Flynn, and D. Deboffle (2004), FTIR and Raman analyses of the Tagish Lake meteorite: Relationship with the aliphatic hydrocarbons observed in the Diffuse Interstellar Medium, *Astron. Astrophys.*, *416*, 983–990.
Mishima, T., T. Hirono, N. Nakamura, W. Tanikawa, W. Soh, and S. Song (2009), Changes to magnetic minerals caused by frictional heating during the 1999 Taiwan Chi-Chi earthquake, *Earth Planets Space*, *61*, 797–801.
Morga, R. (2011), Micro-Raman spectroscopy of carbonized semifusinite and fusinite, *Int. J. Coal Geol.*, *87*, 253–267.
Mukoyoshi, H., A. Sakaguchi, K. Otsuki, T. Hirono, and W. Soh (2006), Co-seismic frictional melting along an out-of-sequence thrust in the Shimanto accretionary complex: Implications on the tsunamigenic potential of splay faults in modern subduction zones, *Earth Planet. Sci. Lett.*, *245*, 330–343.
Nyathi, M. S., C. B. Clifford, and H. H. Schobert (2013), Characterization of graphitic materials prepared from different rank, Pennsylvania anthracites, *Fuel*, *114*, 244–250.
Painter, P. C., M. M. Coleman, R. G. Jenkins, and J. P. L. Walker (1978), Fourier transform infrared study of acid-demineralized coal, *Fuel*, *57*, 125–126.

Painter, P. C., R. W. Snyder, M. Starsinic, M. M. Coleman, D. W. Kuehn, and A. Davis (1981), Concerning the application of FT-infrared to the study of coal: A critical assessment of band assignments and the application of spectral analysis programs, *Appl. Spectrosc.*, *35*, 475–485.
Pandolfo, A. G., R. B. Johns, G. R. Dyrkacz, and A. S. Buchanan (1988), Separation and preliminary characterization of high-purity maceral group fractions from an Australian bituminous coal, *Energy Fuels*, *2*, 657–662.
Pasteris, J. D., and B. Wopenka (1991), Raman spectra of graphite as indicators of degree of metamorphism, *Can. Mineral.*, *29*, 1–9.
Payne, D. F., and P. J. Ortoleva (2001), A model for lignin alteration—Part I: A kinetic reaction-network model, *Org. Geochem.*, *32*, 1073–1085.
Potgieter-Vermaak, R. S., N. Maledi, N. Wagner, J. H. P. Van Heerden, R. Van Grieken, and J. H. Potgietere (2010), Raman spectroscopy for the analysis of coal: A review, *J. Raman Spectrosc.*, *42*, 123–129.
Poutsma, M. K. (1987), *A Review of Thermolysis Studies of Model Compounds Relevant to Processing of Coal*, 225 pp., Oak Ridge Natl. Lab., Oak Ridge, Tenn.
Quirico, E., P. I. Raynal, and M. Bourot-Denise (2003), Metamorphic grade of organic matter in six unequilibrated ordinary chondrites, *Meteorit. Planet. Sci.*, *38*, 795–811.
Quirico, E., G. Montagnac, J. N. Rouzaud, L. Bonal, M. Bourot-Denise, S. Duber, and B. Reynard (2009), Precursor and metamorphic condition effects on Raman spectra of poorly ordered carbonaceous matter in chondrites and coals, *Earth Planet. Sci. Lett.*, *287*, 185–193.
Rahl, J. M., K. M. Anderson, M. T. Brandon, and C. Fassoulas (2005), Raman spectroscopic carbonaceous material thermometry of low-grade metamorphic rocks: Calibration and application to tectonic exhumation in Crete, Greece, *Earth Planet. Sci. Lett.*, *240*, 339–354.
Rochdi, A., and P. Landais (1991), Transmission microinfrared spectroscopy: An efficient tool for microscale characterization of coal, *Fuel*, *70*, 367–371.
Ross, J. V., R. M. Bustin, and J. N. Rouzaud (1991), Graphitization of high rank coals: The role of shear strain: Experimental considerations, *Org. Geochem.*, *17*, 585–596.
Sakaguchi, A. (1996), High geothermal gradient with ridge subduction beneath Cretaceous Shimanto accretionary prism southwest, Japan, *Geology*, *24*, 795–798.
Sakaguchi, A., A. Yanagihara, K. Ujiie, H. Tanaka, and M. Kameyama (2007), Thermal maturity of a fold-thrust belt based on vitrinite reflectance analysis in the Western Foothills complex, western Taiwan, *Tectonophysics*, *443*, 220–232.
Schneider, B., J. Stokr, P. Schmidt, M. Mihailov, S. Dirlikov, and N. Peeva (1979), Stretching and deformation vibrations of CH_2, $C(CH_3)$ and $O(CH_3)$ groups of poly(methyl methacrylate), *Polymer*, *20*, 705–712.
Shin, T., and T. Teng (2001), An overview of the 1999 Chi-Chi, Taiwan, Earthquake, *Bull. Seismol. Soc. Am.*, *91*, 895–913.
Sibson, R. H. (1973), Interaction between temperature and pore-fluid pressure during earthquake faulting—A mechanism for partial or total stress relief, *Nature*, *243*, 66–68.
Sibson, R. H. (1974), Frictional constraints on thrust, wrench and normal faults, *Nature*, *249*, 542–544.
Strezov, V., J. A. Lucas, and L. Strezov (2000), Quantifying the heats of coal devolatilization, *Metall. Mater. Trans. B*, *31*, 1125–1131.
Stuart, B. H. (2004), *Infrared Spectroscopy: Fundamentals and Applications*, 244 pp., John Wiley, Chichester, England, U. K.
Sweeney, J. J., and A. K. Burnham (1990), Evaluation of a simple model of vitrinite reflectance based on chemical kinetics, *AAPG Bull.*, *74*, 1559–1570.
Tanikawa, W., M. Sakaguchi, T. Hirono, W. Lin, W. Soh, and S. Song (2009), Transport properties and dynamic processes in a fault zone from samples recovered from TCDP Hole B of the Taiwan Chelungpu Fault Drilling Project, *Geochem. Geophys. Geosyst.*, *10*, Q04013, doi: 10.1029/2008GC002269.
Tuinstra, F., and J. L. Koenig (1970), Raman spectrum of graphite, *J. Chem. Phys.*, *53*, 1126–1130.
Wender, I. (1976), Catalytic synthesis of chemicals from coal, *Catal. Rev. Sci. Eng.*, *14*, 97–129.
Wopenka, B., and J. D. Pasteris (1993), Structural characterization of kerogens to granulite-facies graphite: Applicability of Raman microprobe spectroscopy, *Am. Mineral.*, *78*, 533–557.
Wu, H., K. Ma, M. Zoback, N. Boness, H. Ito, J. Hung, and S. Hickman (2007), Stress orientations of Taiwan Chelungpu-Fault Drilling Project (TCDP) hole-A as observed from geophysical logs, *Geophys. Res. Lett.*, *34*, L01303, doi:10.1029/2006GL028050.
Xu, T., H. Shi, H. Wang, and X. Huang (2014), Dynamic evolution of emitted volatiles from thermal decomposed bituminous materials, *Constr. Build. Mater.*, *64*, 47–53.
Yui, T. F., E. Huang, and J. Xu (1996), Raman spectrum of carbonaceous, material: A possible metamorphic grade indicator for low grade metamorphic rocks, *J. Metamorph. Geol.*, *14*, 115–124.
Zanetti, J. E., and G. Egloff (1917), The thermal decomposition of benzene, *J. Ind. Eng. Chem.*, *9*, 350–356.
Zeng, Y., and C. Wu (2007), Raman and infrared spectroscopic study of kerogen treated at elevated temperatures and pressures, *Fuel*, *86*, 1192–1200.
Zhou, M., K. Wang, Z. Mena, S. Gao, Z. Li, and C. Sun (2012), Study of high-pressure Raman intensity behavior of aromatic hydrocarbons: Benzene, biphenyl and naphthalene, *Spectrochim. Acta A*, *97*, 526–531.
Zhou, Q., X. Xiao, L. Pan, and H. Tian (2014), The relationship between micro-Raman spectral parameters and reflectance of solid bitumen, *Int. J. Coal Geol.*, *121*, 19–25.
Zickler, G. A., B. Smarsly, N. Gierlinger, H. Peterlik, and O. Paris (2006), A reconsideration of the relationship between the crystallite size L_a of carbons determined by X-ray diffraction and Raman spectroscopy, *Carbon*, *44*, 3239–3246.